JOURNAL OF PETROLOGY | VOLUME 43 | NUMBER 7 | PAGES 1155–1176 | 2002

Between a Hotspot and a Cold Spot: Isotopic Variation in the Southeast Indian Ridge Asthenosphere, 86°E–118°E

J. J. MAHONEY[1]*, D. W. GRAHAM[2], D. M. CHRISTIE[2], K. T. M. JOHNSON[3], L. S. HALL[1] AND D. L. VONDERHAAR[1]

[1]SCHOOL OF OCEAN AND EARTH SCIENCE AND TECHNOLOGY, UNIVERSITY OF HAWAII, HONOLULU, HI 96822, USA
[2]COLLEGE OF OCEANIC AND ATMOSPHERIC SCIENCES, OREGON STATE UNIVERSITY, CORVALLIS, OR 97331, USA
[3]BISHOP MUSEUM, HONOLULU, HI 96817, USA

RECEIVED JULY 13, 2001; REVISED TYPESCRIPT ACCEPTED JANUARY 7, 2002

Glasses from a 2600 km section of the Southeast Indian Ridge west of the Australian–Antarctic Discordance all possess Nd–Pb–Sr isotopic signatures typical of Indian Ocean ridge basalt. The boundary between Pacific- and Indian-Ocean-type ridge basalt within the Discordance thus marks the westernmost extent of shallow Pacific-type asthenosphere beneath the ridge. Along-axis He, Nd, Pb, and Sr isotopic patterns are largely independent of ridge segmentation, but a weak tendency is evident for the most strongly Indian-Ocean-type mantle to be relatively fusible and for shallower asthenosphere to have lower $^{3}He/^{4}He$. On average, ε_{Nd} appears slightly lower than for ridges in the western Indian Ocean far from hotspots. Importantly, the regional isotopic patterns cannot be explained by a previously proposed eastward flow of Kerguelen–Heard or Amsterdam–St. Paul hotspot mantle. Nd, Pb and (to a much lesser extent) Sr isotopes correlate roughly with many incompatible element ratios, including parent–daughter ratios. If interpreted as mantle errorchrons, the latter correlations imply 'ages' of 200–300 Ma, significantly greater than the oldest known age of the Kerguelen–Heard hotspot (119–135 Ma) commonly postulated to have played an important role in creating the isotopic signature of Indian Ocean mantle. Rather than reflecting relatively recent mixing involving mantle from hotspots in the region, much of the observed isotopic heterogeneity may be the result of other mixing or of past intra-mantle chemical fractionation, probably associated with melting.

KEY WORDS: *Southeast Indian Ridge; isotopes and trace elements; mantle geochemistry; Indian Ocean hotspots*

INTRODUCTION

Until recently, the 3200 km section of the Southeast Indian Ridge (SEIR) between the Amsterdam–St. Paul hotspot and the Australian–Antarctic Discordance (AAD) remained the largest unsampled portion of the Indian Ocean ridge system (Fig. 1). In the eastern 2600 km of this region, between 86°E and 118°E, spreading rate is nearly constant at 69–75 mm/yr and axial depth increases from west to east by more than 2300 m, indicating a gradual eastward decrease in upper mantle temperature of at least 60–110°C (e.g. Sempéré *et al.*, 1997). This along-axis temperature gradient has been theorized to correspond to a large-scale eastward flow (and gradual dilution) of mantle emanating from the Amsterdam–St. Paul and/or Kerguelen–Heard hotspots toward a region of unusually cool asthenosphere, sometimes termed a 'cold spot', beneath the AAD at 120–128°E (e.g. Marks *et al.*, 1991; Sempéré *et al.*, 1997). An even broader role for the Kerguelen–Heard hotspot has been proposed by several workers (e.g. Storey *et al.*, 1989; Mahoney *et al.*, 1992; Weis & Frey, 1996), who have suggested that this hotspot was important in the origin of the distinctive isotopic signature of mid-ocean ridge basalt (MORB) in the Indian Ocean, Indian MORB being characterized in particular by lower $^{206}Pb/^{204}Pb$ relative to $^{208}Pb/^{204}Pb$, ε_{Nd}, and $^{87}Sr/^{86}Sr$ than Pacific and North Atlantic MORB, and by comparatively low ε_{Nd} and high $^{87}Sr/^{86}Sr$ (e.g. Hedge *et al.*, 1979; Hamelin *et al.*, 1986; Michard *et al.*, 1986; Dosso *et al.*, 1988; Mahoney *et al.*, 1989, 1992;

*Corresponding author. Telephone: 1-808-956-8705. Fax: 1-808-956-5512. E-mail: jmahoney@soest.hawaii.edu

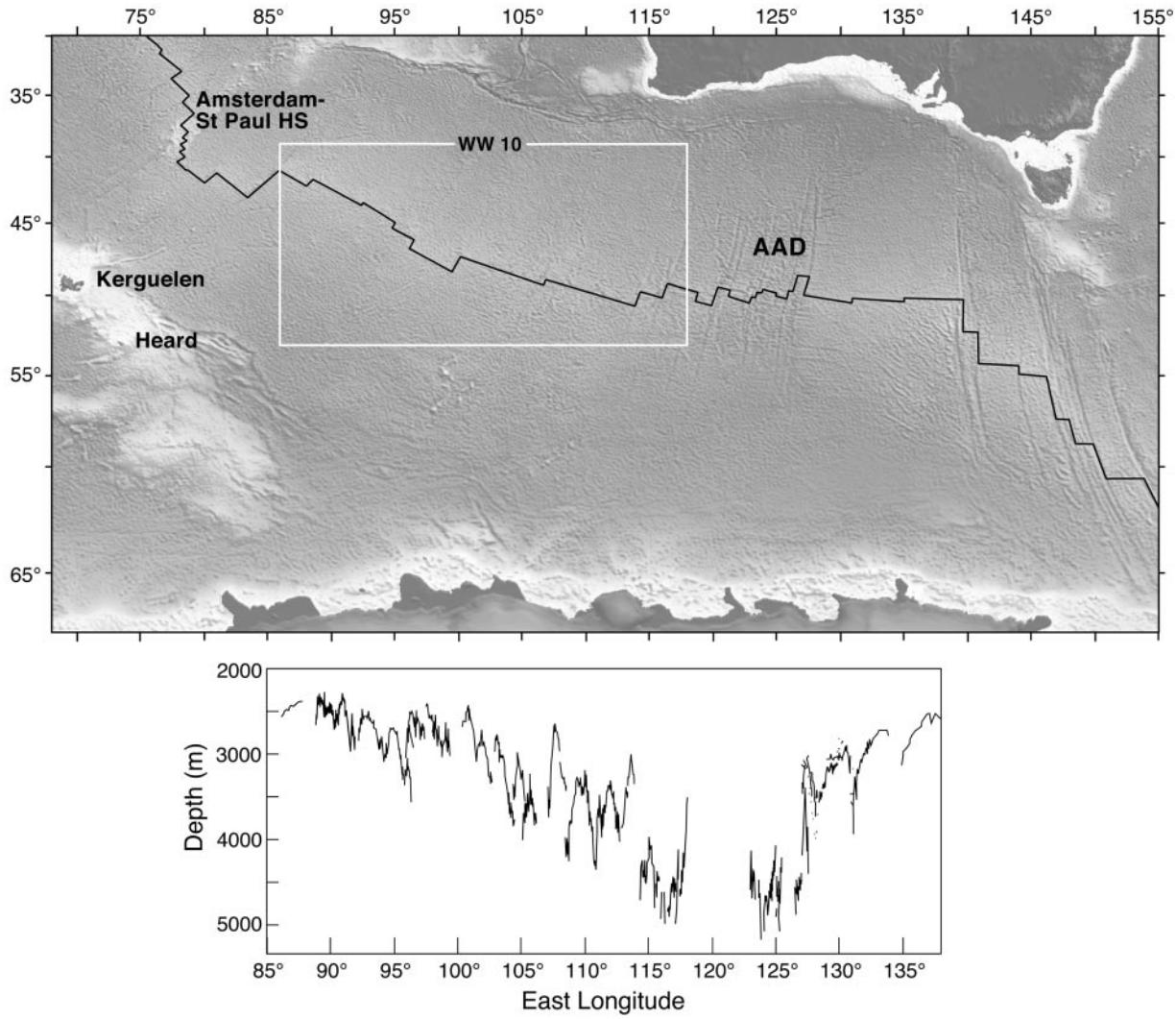

Fig. 1. Top: map of the southeastern Indian Ocean, after Smith & Sandwell (1997). The box indicates the 86–118°E portion of the SEIR; the position of the ridge axis is shown by the black line. HS, hotspot. Bottom: axial depth vs longitude in the study area and AAD (Australian–Antarctic Discordance) from Sempéré *et al.* (1997), West *et al.* (1997) and Scheirer *et al.* (2000).

Rehkämper & Hofmann, 1997). Within the AAD near 126°E, isotopic studies have revealed the existence of an abrupt transition, occurring over <40 km along-axis, between Indian-MORB-type and Pacific-MORB-type mantle (Klein *et al.*, 1988; Pyle *et al.*, 1992). This boundary has been migrating westward for at least the last several million years and perhaps for the last several tens of millions of years (Pyle *et al.*, 1992, 1995; Christie *et al.*, 1998). However, whether this boundary represents *the* boundary between these two enormous domains of MORB-type mantle or only *a* boundary, with, for example, interfingering of the two types along-axis farther to the west, has remained unknown because of the lack of any samples from the long stretch of ridge west of the AAD.

In 1995 and 1996, respectively, the Westward 10 and Boomerang 6 expeditions of the R.V. *Melville* recovered basalts from 197 sites along the SEIR between 77°E and 118°E (Christie *et al.*, 1995; Johnson *et al.*, 1996). In this paper we report He, Sr, Pb, and Nd isotopic results and selected elemental data for glasses from the section of ridge between 86°E and 118°E, and discuss implications for asthenospheric flow and geochemical evolution in the southeastern Indian Ocean mantle.

SAMPLES AND METHODS

With the exception of two dredge hauls from near-axis seamounts and one (*WW10*-116, where *WW* indicates

Westward) from a transform-fault high between two spreading segments, the 71 glasses we analyzed isotopically were taken from, or very close to, the active spreading axis, as defined by combined bathymetric and geophysical data (Christie *et al.*, 1995; Johnson *et al.*, 1996; Sempéré *et al.*, 1997; Scheirer *et al.*, 2000). Elemental data for a much larger number of samples (Douglas-Priebe, 1998; Christie *et al.*, in preparation; K. T. M. Johnson, unpublished data, 2000) show that most of the lavas in the collection are normal, or N-type, MORB, although many, particularly abundant throughout the eastern two-thirds of the study area where the axial depth gradient is slightly steeper, are more enriched in highly incompatible elements relative to moderately incompatible elements than are N-MORB. Here, we refer to lavas with chondrite-normalized La/Sm, $(La/Sm)_n$, >0·8 and/or K_2O/TiO_2 >0·15 as E-type MORB, although we emphasize that a continuum of compositions exists. Compositional heterogeneity at small scales is demonstrated by the fact that many of the dredge hauls containing E-MORB also contain N-MORB (Douglas-Priebe, 1998; Christie *et al.*, in preparation).

Samples we analyzed isotopically were chosen to ensure a relatively uniform geographic coverage of the axis, within the limitations imposed by dredge and wax-core locations and availability of sufficient fresh glass. Additionally, we analyzed two samples from each of five individual dredge sites to assess the range of isotopic variability associated with intra-dredge-scale elemental heterogeneity. Processing and analysis of samples followed our normal procedures for MORB glasses (e.g. Pyle *et al.*, 1992; Mahoney *et al.*, 1994; Graham *et al.*, 1999; Christie *et al.*, in preparation). Isotopic fractionation corrections, standard reference values, procedural blanks, and analytical uncertainties are summarized in the Table 1 footnotes. Major and trace element data used in the figures and discussed below are presented in Table 2. A comprehensive suite of major and trace elements has been measured for a much more extensive set of 86–118°E glasses by Douglas-Priebe (1998), Christie *et al.* (in preparation), and K. T. M. Johnson *et al.* (unpublished data, 2000) using electron microprobe and inductively coupled plasma–mass spectrometric methods.

RESULTS

Isotopic data

Our most fundamental result is that all of the samples analyzed are of the Indian MORB type. As with MORB from the Indian Ocean farther west, the 86–118°E data lie to the low-$^{206}Pb/^{204}Pb$, low-ε_{Nd}, high-$^{87}Sr/^{86}Sr$ side of the isotopic fields defined by >95% of Pacific and North Atlantic MORB in Fig. 2a, b and d. The Indian-MORB nature of the lavas is demonstrated perhaps most graphically in the profile of Δ8/4 vs longitude in Fig. 3a [Δ8/4 is a measure of the vertical distance of a data point from a line fitted through the Pacific and North Atlantic MORB array in Fig. 2a; see Hart (1984) for the relevant equations]. For nearly all Pacific MORB Δ8/4 <20, whereas Δ8/4 >20 for virtually all Indian MORB (e.g. Mahoney *et al.*, 1992, and references therein); Δ8/4 for the 86–118°E SEIR glasses ranges from 23 to 72.

A substantial range of isotopic values is present in our dataset (Table 1); $^{206}Pb/^{204}Pb$ varies from 17·362 to 18·494, $^{87}Sr/^{86}Sr$ from 0·70271 to 0·70368, ε_{Nd} from +4·2 to +9·8, and $^{3}He/^{4}He$ from 6·53 to 9·70 R_A (where R_A is the atmospheric ratio). Isotopic values for the few seamount glasses that have been analyzed are within the range defined by nearby axial lavas. Within-dredge Nd–Sr–Pb isotopic heterogeneity varies from almost negligible in dredges *WW10*-116 and -138 to a significant fraction of the total range observed in the entire 86–118°E region in dredges *WW10*-128 and -145, in which chemical differences are also pronounced. The two samples analyzed from *WW10*-128, for example, differ by 4·4 ε_{Nd} units, by 0·0004 in $^{87}Sr/^{86}Sr$, and by 0·4 in $^{206}Pb/^{204}Pb$. In both of these dredges, the more incompatible-element-enriched glasses have the lower ε_{Nd} and the higher Sr and Pb isotopic values. In the 86–118°E region overall, the Nd–Sr–Pb isotopic data for E-MORB and N-MORB overlap considerably but the N-MORB range to lower $^{87}Sr/^{86}Sr$, whereas the E-MORB tend to have higher Pb isotope ratios. Among E- and N-MORB from adjacent sampling stations, the E-MORB have similar to lower ε_{Nd} and similar to higher $^{87}Sr/^{86}Sr$, Pb isotope ratios, and Δ8/4 (Fig. 3; note the reversed ε_{Nd} scale in Fig. 3f). With the exception of dredge *WW10*-89, the E-MORB have low $^{3}He/^{4}He$, between 6·53 and 7·36 R_A, whereas the N-MORB vary over nearly the entire range observed, from 6·68 to 9·70 R_A. In dredges *WW10*-128 and *WW10*-145, for each of which we analyzed He isotopes in two different samples having significantly different $(La/Sm)_n$, the more incompatible-element-enriched glass has lower $^{3}He/^{4}He$ (by 0·57 and 0·67 R_A, respectively). Overall, however, no systematic difference in He isotopes is apparent between E- and N-MORB from adjacent stations (Fig. 3d).

Our results support previous indications of large-scale isotopic provinciality within the Indian Ocean ridge system (Mahoney *et al.*, 1989, 1992; Pyle *et al.*, 1992). The great majority of the 86–118°E samples, for example, have $^{206}Pb/^{204}Pb$ clustering between 17·8 and 18·3. Within this same range of $^{206}Pb/^{204}Pb$, and excluding segments near hotspots, basalts of the central–eastern Southwest Indian Ridge and the Carlsberg and Central Indian Ridge system in the western Indian Ocean have distinctly higher average ε_{Nd} values (the average for each is +8·7) than do the 86–118°E SEIR lavas (average

Table 1: Isotopic data for Southeast Indian Ridge glasses, 86–118°E

Sample	N or E	°E	°S	Depth (m)	$^{87}Sr/^{86}Sr$	$^{143}Nd/^{144}Nd$	ε_{Nd}	$^{206}Pb/^{204}Pb$	$^{207}Pb/^{204}Pb$	$^{208}Pb/^{204}Pb$	Δ8/4 (R/R_A)	$^{3}He/^{4}He$	[He]
BM06-36-1	N	86·23	41·10	2500	0·70348	0·512943	5·9	17·735	15·487	37·760	69·1	8·50	0·88
BM06-35-8	N	86·63	41·32	2560								8·86	0·306
BM06-34-1	N	87·09	41·52	2480	0·70358	0·512904	5·1	17·812	15·497	37·886	72·4	8·90	6·21
BM06-33-2	N	88·04	42·12	2450	0·70364	0·512889	4·9	17·970	15·501	37·979	62·6	9·70	16·32
WW10-69-1	N	88·92	41·87	2353	0·70331	0·512954	6·1	18·030	15·473	37·892	46·7	9·14	3·70
WW10-66-18	N, smt	89·32	41·72	1570	0·70337	0·512949	6·1	18·173	15·492	38·013	41·5		
WW10-70-32	N	90·20	42·57	2575	0·70302	0·513021	7·4	17·910	15·474	37·646	36·6	8·61	11·78
WW10-71-1	N	90·80	42·89	2350	0·70293	0·513040	7·8	17·863	15·479	37·456	23·3	8·02	5·45
WW10-65-9	N	91·09	43·08	2494	0·70302	0·513038	7·8	17·868	15·480	37·564	33·5	8·35	2·30
WW10-72-2	N, smt	91·29	43·42	1605	0·70298	0·513029	7·6	17·970	15·464	37·661	30·8	8·21	
WW10-73-8	N	91·68	43·47	2738	0·70302	0·513032	7·6	17·868	15·485	37·569	34·0	8·24	1·85
WW10-74-2	N	92·33	43·43	2560	0·70314	0·513016	7·3	17·848	15·464	37·549	34·4		
WW10-75-4	N	92·68	43·58	2585	0·70324	0·512995	6·9	17·844	15·478	37·547	34·7	8·37	10·72
WW10-76-1	N	93·11	43·88	2653	0·70332	0·512961	6·3	17·874	15·484	37·586	34·9	8·46	12·33
WW10-77-7	N	93·77	44·12	2795	0·70292	0·513060	8·2	17·793	15·465	37·443	30·4	8·34	7·74
WW10-78-2	N	94·83	44·83	2719	0·70312	0·513012	7·3	17·871	15·489	37·537	30·4	7·71	11·41
WW10-79-17	N	95·41	45·11	3045	0·70304	0·513018	7·4	17·875	15·477	37·523	28·5		
WW10-81-1	N	95·59	45·17	3190	0·70305	0·513011	7·2	17·883	15·479	37·546	29·8	7·81	0·54
WW10-82-35	N	95·70	45·18	3164	0·70311	0·513018	7·4	17·926	15·479	37·550	25·0	7·75	10·40
WW10-83-17	E	95·76	45·05	3069	0·70320	0·512986	6·7	18·133	15·504	37·920	37·0		
WW10-84-7	N	95·93	45·11	2660	0·70308	0·513036	7·7	17·754	15·463	37·498	40·6	8·08	4·44
WW10-WC48	E	95·93	46·09	2990	0·70309	0·512963	6·3	18·494	15·519	38·250	26·4	7·31	0·99
WW10-87-38	N	96·37	46·78	2520	0·70323	0·512981	6·7	17·731	15·470	37·596	53·2	8·37	0·88
WW10-88-1	N	96·83	47·08	2568	0·70314	0·513015	7·3	17·841	15·481	37·786	58·9	9·38	6·30
WW10-89-4	E	97·51	47·45	2470	0·70361	0·512911	5·3	17·937	15·499	37·801	48·8	8·08	1·65
WW10-89-107	E	97·51	47·45	2470	0·70339	0·512952	6·1	17·859	15·492	37·743	52·4	8·33	4·05
WW10-90-1	N	98·16	47·71	2607	0·70308	0·512960	6·2	17·843	15·483	37·614	41·5	7·90	10·45
WW10-91-3	N	98·60	47·91	2900	0·70315	0·512986	6·7	17·914	15·483	37·682	39·7	7·92	1·83
WW10-92-1	N	98·94	48·10	2668	0·70317	0·513019	7·4	17·891	15·486	37·578	32·1	7·82	2·28
WW10-96-1	E	100·67	47·34	2465	0·70301	0·513001	7·0	18·133	15·483	37·923	37·3	7·36	2·74
WW10-97-8	E	100·86	47·19	2015	0·70284	0·513018	7·4	18·088	15·466	37·874	37·9		
WW10-98-3	E	100·96	47·46	2583	0·70301	0·512988	6·8	18·257	15·512	38·102	40·2	7·33	3·78
WW10-99-15	N	101·22	47·59	2842	0·70293	0·513020	7·4	17·996	15·467	37·764	38·0		
WW10-100-1	E	101·53	47·63	2857	0·70306	0·512978	6·6	18·105	15·485	37·944	42·8	7·32	17·77
WW10-102-1	N	102·14	47·88	2986	0·70293	0·513021	7·4	17·989	15·475	37·770	39·4		
WW10-103-4	N	102·54	48·02	3230	0·70291	0·513039	7·8	17·951	15·465	37·719	38·9	7·18	3·76
WW10-105-1	E	103·04	47·77	2783	0·70290	0·513047	7·9	17·987	15·480	37·802	42·9		
WW10-106-4	E	103·25	47·90	2985	0·70290	0·513015	7·3	18·114	15·477	37·922	39·5	7·12	13·82
WW10-108-3	E	103·57	47·97	3080	0·70293	0·513024	7·5	18·103	15·482	37·936	42·2		
WW10-110-4	N	103·93	48·10	3480	0·70286	0·513028	7·6	18·062	15·466	37·844	38·0	7·25	4·65
WW10-111-18	E	104·66	48·21	3070	0·70312	0·512934	5·7	18·322	15·506	38·217	43·9	7·16	12·54
WW10-112-1	E	104·97	48·32	3163	0·70304	0·512985	6·7	18·140	15·494	37·990	43·2		
WW10-113-7	N	105·22	48·75	3630	0·70274	0·513052	8·0	18·144	15·467	37·935	37·2	6·82	0·83
WW10-114-12	E*	105·59	49·12	2875	0·70351	0·512857	4·2	18·351	15·536	38·268	45·5	7·36	4·84
WW10-115-3	E	105·87	49·23	3636	0·70311	0·512992	6·9	18·060	15·495	38·005	54·3	6·80	7·52
WW10-116-2	E	106·49	48·87	4835	0·70294	0·513007	7·2	18·233	15·487	38·175	50·4		

Sample	N or E	°E	°S	Depth (m)	$^{87}Sr/^{86}Sr$	$^{143}Nd/^{144}Nd$	ε_{Nd}	$^{206}Pb/^{204}Pb$	$^{207}Pb/^{204}Pb$	$^{208}Pb/^{204}Pb$	$\Delta 8/4$ (R/R_A)	$^{3}He/^{4}He$	[He]
WW10-116-15	E	106·49	48·87	4835	0·70290	0·513008	7·2	18·251	15·500	38·223	53·1	6·82	3·24
WW10-117-1	E	107·15	48·35	3520	0·70289	0·513011	7·2	18·284	15·508	38·249	51·7	6·88	8·78
WW10-118-1	E	107·53	48·43	2673	0·70301	0·512973	6·5	18·365	15·503	38·353	52·3	6·80	6·48
WW10-122-1	E	108·28	48·74	3277	0·70298	0·512972	6·5	18·282	15·491	38·273	54·3	6·65	2·11
WW10-124-1	N	108·51	49·03	3935	0·70273	0·513041	7·8	18·011	15·459	37·845	44·3	6·83	3·53
WW10-125-1	N	109·11	49·45	3475	0·70285	0·513023	7·5	18·128	15·475	38·047	50·3	6·68	15·94
WW10-126-7	E	109·48	49·53	3240	0·70336	0·512909	5·2	18·198	15·512	38·262	63·4	7·07	6·49
WW10-128-1	E	110·41	49·83	3745	0·70343	0·512917	5·4	18·132	15·533	38·193	64·4	7·13	0·64
WW10-128-18	N	110·41	49·83	3745	0·70273	0·513141	9·8	17·734	15·449	37·631	56·4	7·70	5·81
WW10-130-1	N	111·13	49·78	3520	0·70274	0·513057	8·1	18·064	15·468	37·964	49·8	7·30	6·89
WW10-132-1	E	111·78	50·21	3328	0·70287	0·513036	7·7	17·972	15·478	37·829	47·4		
WW10-133-1	N	112·40	50·32	3484	0·70271	0·513071	8·4	17·813	15·443	37·594	43·1		
WW10-134-1	N	112·49	50·30	3650	0·70285	0·513040	7·8	17·964	15·454	37·819	47·4	7·20	11·97
WW10-135-8	N	112·59	50·31	3748	0·70281	0·513055	8·1	17·931	15·455	37·785	47·9	7·20	15·30
WW10-136-15	N	112·69	50·32	3842	0·70283	0·513044	7·9	17·950	15·466	37·821	49·2		
WW10-138-1	N	112·86	50·19	3845	0·70289	0·513035	7·7	17·968	15·443	37·722	37·2	7·28	11·60
WW10-138-36	E	112·86	50·19	3845	0·70298	0·513012	7·3	17·952	15·466	37·791	46·0		
WW10-140-5	E	113·45	50·30	3320	0·70292	0·513018	7·4	18·017	15·450	37·810	40·0	7·26	0·52
WW10-141-1	E	113·62	50·35	3002	0·70297	0·512999	7·0	17·947	15·461	37·796	47·1	7·35	3·04
WW10-142-1	N	114·48	49·86	4300	0·70308	0·513015	7·3	17·935	15·479	37·938	62·8		
WW10-144-4	N	115·21	50·01	3997	0·70315	0·513011	7·2	17·894	15·459	37·887	62·6	6·84	8·09
WW10-145-1	E	116·72	49·27	4665	0·70368	0·512929	5·6	17·594	15·473	37·612	71·4	6·53	15·80
WW10-145-7	E	116·72	49·27	4665	0·70311	0·513075	8·5	17·362	15·443	37·320	70·2	7·20	2·52
WW10-146-1	E	117·18	49·51	4818	0·70318	0·512991	6·8	17·974	15·513	38·027	66·9	6·65	5·02
WW10-147-6	E	117·52	49·70	4633	0·70295	0·513018	7·4	18·011	15·470	37·847	44·5		

*Dredge *WW10*-114 was taken on a small, elongate, axis-parallel volcano in an area where the location of the active spreading axis is uncertain; the volcano may mark the location of the axis, or may be a small seamount slightly off-axis. *BM06* and *WW10* prefixes indicate Boomerang 6 and Westward 10 samples. N, E, and smt indicate N-MORB, E-MORB, and seamount. Data are reported relative to values of $^{87}Sr/^{86}Sr = 0{\cdot}71024$ for NBS 987 Sr, $^{143}Nd/^{144}Nd = 0{\cdot}511850$ for La Jolla Nd, and the Pb isotope values of Todt *et al.* (1996) for NBS 981 Pb. The total range measured for NBS 987 Sr over a 2 year period was $\pm 0{\cdot}00002$; for La Jolla Nd it was $\pm 0{\cdot}000011$ (0·2 ε_{Nd} units); for NBS 981 Pb it was $\pm 0{\cdot}011$ for $^{206}Pb/^{204}Pb$, $\pm 0{\cdot}010$ for $^{207}Pb/^{204}Pb$, and $\pm 0{\cdot}031$ for $^{208}Pb/^{204}Pb$. Within-run errors on the isotopic data above are less than or equal to the external uncertainties on these standards. See Hart (1984) for equations for $\Delta 8/4$. Errors (2σ) on He isotope ratios are between 0·03 and 0·06, except for one measurement with an error of 0·08. Helium concentrations ([He]) are in units of micro cc STP/g. Total procedural blanks are 4–32 pg for Pb, <60 pg for Sr, <15 pg for Nd. Blank for He is $<2 \times 10^{-10}$ cm^3 of ^{4}He. Note that $\varepsilon_{Nd} = 0$ corresponds to $^{143}Nd/^{144}Nd = 0{\cdot}51264$.

+7·1; see Fig. 4b). In contrast, lavas from the SEIR NW of Amsterdam and St. Paul islands, and from within the Indian-MORB section of the AAD to as far east as 125°E have similar ε_{Nd} values to those of the 86–118°E glasses (Fig. 4a). Thus, most of the SEIR appears distinct from large portions of the more westerly ridges. This difference, if confirmed by future sampling, could be an original feature of the Indian MORB mantle domain itself, or could reflect comparatively recent differences in hotspot or other components added to, and variably mixed within, large subdomains of the Indian Ocean asthenosphere.

As with other long sections of the Indian Ocean ridge system, correlations among Pb and Nd, and Pb and Sr isotopic ratios are poor (Fig. 2b and d). Pb–Pb isotope correlations (Fig. 2a and c) are somewhat better but still poorer than in many parts of the oceans; among the N-MORB only, $^{207}Pb/^{204}Pb$ and $^{206}Pb/^{204}Pb$ show virtually no correlation. Moreover, the general or large-scale shapes of the longitudinal patterns of Pb, Sr, Nd, and He isotopes differ significantly from each other (Fig. 3). For example, a broad peak is evident in $^{206}Pb/^{204}Pb$, culminating at 107·5°E; this pattern is matched roughly

Table 2: Selected elemental data for Southeast Indian Ridge glasses, 86–118°E

Sample	N or E	Na_8	Fe_8	*mg*-no.	Rb	Ba	Th	U	Nb	La	Sr	Nd	Pb	Sm
BM06-36-1	N	2·60	9·61	59·9		15·2			3·39	4·03	126	12·0	*0·824*	4·34
BM06-34-1	N	2·64	9·75	55·9		16·6			3·37	4·16	152	12·1	*0·803*	4·42
BM06-33-1	N	2·65	9·37	63·6		7·8			2·50	3·27	138	10·1	*0·605*	3·73
WW10-69-1	N	2·93	11·3	73·4	0·29	4·4	0·050	0·019	0·738	1·40	100	4·77	0·193	1·79
WW10-66-18	N, smt	2·88	9·64	63·7	0·48	6·7	0·072	0·044	1·68	2·58	119	8·33	*0·440*	2·89
WW10-70-32	N	2·56	9·85	63·3	0·79	11·4	0·108	0·057	2·55	3·46	118	10·6	*0·542*	3·58
WW10-71-1	N	2·89	9·12	67·6	0·84	19·1	0·112	0·039	2·30	3·26	139	9·45	0·448	3·30
WW10-65-9	N	2·54	9·60	63·8	1·28	19·0	0·154	0·073	2·93	3·62	115	10·9	*0·445*	3·74
WW10-72-2	N, smt	2·59	9·39	65·6	0·32	5·5	0·063	0·021	1·03	1·85	87·8	6·60	*0·260*	2·37
WW10-73-8	N	2·61	9·20	61·2	0·95	17·5	0·140	0·064	2·70	4·06	119	12·1	0·584	4·27
WW10-74-2	N	2·84	8·38	63·3	1·48	27·4	0·214	0·072	3·69	4·49	152	11·8	*0·608*	3·76
WW10-75-4	N	3·09	8·72	64·5	1·19	21·0	0·134	0·061	3·12	3·58	140	10·1	0·478	3·31
WW10-76-1	N	2·88	8·55	64·5	1·77	31·4	0·187	0·081	3·98	4·42	167	11·2	0·552	3·55
WW10-77-7	N	2·62	8·94	62·5	0·95	14·1	0·177	0·068	2·78	4·17	106	12·7	*0·552*	4·36
WW10-78-2	N	2·80	8·81	68·4	0·90	18·2	0·111	0·053	2·42	3·08	131	8·38	0·401	2·85
WW10-79-17	N	2·74	9·15	66·6	0·94	15·4	0·096	0·055	2·72	3·65	128	11·5	*0·547*	4·00
WW10-81-1	N	2·63	8·79	65·1	0·78	14·2	0·104	0·044	2·16	3·02	124	8·83	*0·382*	3·00
WW10-82-35	N	2·75	9·72	67·7	0·93	15·0	0·067	0·051	2·51	3·13	110	9·24	0·395	3·12
WW10-83-17	E	3·16	7·98	70·0	4·59	57·0	0·575	0·186	9·33	6·22	190	9·49	*0·568*	2·74
WW10-84-7	N	2·97	8·56	69·0	0·96	13·6	0·125	0·057	2·74	3·41	152	9·69	*0·467*	3·26
WW10-WC48	E	2·98	7·45	69·9	10·6	127	1·36	0·478	20·4	12·6	272	14·7	*0·853*	3·73
WW10-87-38	N	2·79	9·22	66·4	0·73	10·2	0·141	0·044	1·70	2·64	122	8·31	*0·426*	2·99
WW10-88-1	N	2·54	9·42	68·2	0·40	5·2	0·086	0·024	1·12	1·99	75·1	6·53	*0·280*	2·41
WW10-89-4	E	3·08	8·76	67·6	3·75	53·5	0·558	0·209	9·22	7·57	232	13·0	*0·966*	3·84
WW10-89-107	E	2·93	7·95	66·5	2·45	32·9	0·428	0·149	5·78	5·60	204	11·4	*0·757*	3·51
WW10-90-1	N	2·92	9·28	61·2	0·72	9·9	0·157	0·067	2·45	3·74	149	9·82	*0·477*	3·32
WW10-91-3	N	2·56	9·53	56·9	3·13	34·6	0·396	0·168	7·32	6·95	125	17·6	*0·909*	5·81
WW10-92-1	N	2·77	9·38	68·7	1·53	21·2	0·144	0·069	3·13	3·08	122	8·47	*0·493*	2·90
WW10-96-1	E	2·87	8·65	61·1	2·79	31·2	0·433	0·155	6·57	5·77	147	12·2	*0·646*	3·81
WW10-97-8	E	3·52	9·27	71·7	0·84	11·3	0·133	0·059	2·43	3·52	195	8·92	*0·447*	2·75
WW10-98-3	E	2·74	8·91	65·6	3·53	37·6	0·552	0·162	6·81	5·34	164	9·84	*0·518*	3·06
WW10-99-15	N	2·73	8·74	63·4	1·40	16·4	0·220	0·087	3·58	4·00	132	10·0	*0·608*	3·30
WW10-100-1	E	2·83	8·60	65·3	3·48	40·5	0·521	0·159	7·67	6·40	144	12·1	0·660	3·64
WW10-102-1	N	2·65	9·04	66·7	1·00	11·7	0·131	0·055	2·45	2·89	112	8·34	*0·406*	2·85
WW10-103-4	N	2·79	9·44	70·4	0·92	10·3	0·102	0·045	2·05	2·38	106	6·81	*0·336*	2·36
WW10-105-1	E	3·13	7·97	65·2	1·50	18·1	0·236	0·086	4·02	4·74	165	10·6	*0·609*	3·32
WW10-106-4	E	2·76	9·13	68·8	1·25	16·0	0·164	0·061	3·25	3·17	123	7·31	0·410	2·38
WW10-108-3	E	2·70	9·17	70·3	1·23	16·4	0·221	0·078	3·05	3·51	116	7·85	*0·361*	2·66
WW10-110-4	N	2·57	8·93	67·1	0·78	9·6	0·132	0·045	2·12	2·69	95·8	7·52	0·324	2·65
WW10-111-18	E	3·10	7·07	65·7	4·76	57·7	0·760	0·236	10·8	8·59	209	13·8	0·820	3·88
WW10-112-1	E	2·83	8·58	67·9	1·52	19·6	0·274	0·086	3·62	4·01	115	8·94	*0·498*	2·91
WW10-113-7	N	2·65	8·66	65·0	1·66	19·6	0·218	0·074	3·85	3·94	114	9·95	0·429	3·27
WW10-114-12	E	3·08	7·30	69·5	11·5	142	1·40	0·388	21·1	11·6	301	14·4	*0·890*	3·72
WW10-115-3	E	3·36	9·22	69·2	2·44	28·1	0·376	0·104	4·76	4·67	113	10·1	0·607	3·27
WW10-116-2	E	3·36	9·70	69·0	5·54	60·2	0·798	0·215	9·79	7·16	141	12·5	*0·654*	3·79
WW10-116-15	E	3·36	9·47	71·3	4·86	52·9	0·630	0·197	9·37	6·99	144	12·6	0·611	3·84
WW10-117-1	E	3·07	7·64	61·9	4·24	49·2	0·628	0·189	8·55	7·36	151	14·5	0·716	4·40

Sample	N or E	Na_8	Fe_8	*mg*-no.	Rb	Ba	Th	U	Nb	La	Sr	Nd	Pb	Sm
WW10-118-1	E	2·97	7·17	59·8	7·59	80·3	1·03	0·299	13·9	10·5	204	17·9	0·939	5·18
WW10-122-1	E	2·89	7·70	60·0	3·52	38·0	0·529	0·162	7·25	6·96	132	14·9	0·724	4·60
WW10-124-1	N	2·76	9·43	69·1	0·32	3·6	0·025	0·019	1·10	1·98	92	6·38	0·288	2·33
WW10-125-1	N	2·84	8·50	68·2	0·93	10·4	0·109	0·049	2·43	3·00	118	7·96	0·370	2·64
WW10-126-7	E	3·25	7·94	69·6	8·39	95·6	1·15	0·289	13·0	9·64	243	12·8	0·989	3·48
WW10-128-1	E	2·97	9·63	70·3	4·70	51·1	0·606	0·159	7·04	5·40	150	8·33	*0·600*	2·62
WW10-128-18	N	3·15	10·3	74·6	0·93	9·47	0·157	0·035	1·29	1·87	107	5·51	*0·273*	1·95
WW10-130-1	N	3·07	8·55	66·3	0·85	9·5	0·092	0·042	1·80	2·90	133	8·77	0·478	2·95
WW10-132-1	E	3·05	8·11	66·9	2·08	22·2	0·245	0·075	3·61	4·38	168	10·7	*0·561*	3·29
WW10-133-1	N	3·00	9·19	68·1	1·21	12·2	0·142	0·048	2·01	3·07	129	9·19	*0·435*	3·12
WW10-134-1	N	2·82	9·88	67·3	1·57	16·5	0·186	0·056	2·56	3·28	97·6	9·16	*0·364*	3·13
WW10-135-8	N	2·82	9·60	64·1	1·74	16·8	0·206	0·056	3·08	3·80	104	10·9	0·464	3·73
WW10-136-15	N	2·84	9·45	66·3	1·57	15·3	0·185	0·063	2·94	3·55	108	9·94	*0·425*	3·40
WW10-138-1	N	2·76	9·55	60·4	2·19	21·5	0·322	0·114	5·21	5·78	115	16·0	0·662	5·24
WW10-138-36	E	2·75	8·45	66·8	1·93	25·4	0·304	0·084	4·32	4·27	127	9·26	*0·480*	3·01
WW10-140-5	E	2·73	8·41	59·8	2·43	26·1	0·355	0·122	5·36	5·54	137	13·0	*0·596*	4·13
WW10-141-1	E	2·87	8·21	61·8	2·98	33·2	0·388	0·129	6·26	5·73	144	12·7	0·617	4·05
WW10-142-1	N	3·04	8·41	67·9	1·70	18·2	0·214	0·069	3·62	4·15	130	10·3	*0·534*	3·41
WW10-144-4	N	2·91	8·46	69·2	1·44	16·0	0·188	0·060	3·06	3·55	118	8·91	0·514	2·96
WW10-145-1	E	3·58	6·53	71·5	6·10	69·9	0·634	0·183	8·59	6·11	204	10·6	*0·830*	3·19
WW10-145-7	E	3·59	6·71	69·3	2·78	32·0	0·332	0·110	4·08	4·59	203	9·49	*0·729*	2·91
WW10-146-1	E	3·25	7·44	71·0	1·97	20·7	0·236	0·071	3·44	3·97	135	9·31	0·605	2·97
WW10-147-6	E	2·82	8·08	59·4	2·59	25·2	0·396	0·133	6·01	6·60	127	16·6	*0·913*	5·31
BHVO-1(meas.)					10·4	144	1·17	0·46	19·8	15·4	396	24·6	2·15	6·16
BHVO-1(rec.)					11·0	139	1·23	0·42	19·0	15·8	403	25·2	2·05	6·20

Na_8, Fe_8, and *mg*-number are glass-group averages from Douglas-Priebe (1998) and Christie *et al.* (in preparation). *mg*-number = 100[Mg/(Mg + Fe^{2+})] (atomic), assuming 85% of iron is in the 2+ oxidation state. The Fe, Na, and Mg oxide abundances (in wt %; relative uncertainty 0·5%) were measured by electron microprobe at Oregon State University. Trace element abundances (in ppm) were measured by inductively coupled plasma mass spectrometry at Oregon State University; precision is 1–5%. About two-thirds of the Pb abundance measurements (in italics) were made by isotope dilution at the University of Hawaii; external analytical uncertainty is 0·5%. Comparison of measured and recommended [mostly from Govindaraju (1994)] trace element values for standard BHVO-1 provides an indication of accuracy.

by $^{208}Pb/^{204}Pb$. However, it is not matched by $^{207}Pb/^{204}Pb$ (not shown) or by $\Delta 8/4$, which instead shows a broad overall increase from 90°E to 116·7°E. Nor is it matched by peaks or depressions in the Nd or Sr isotope patterns, although it does correspond approximately to a local minimum in $^{3}He/^{4}He$. The Sr isotope ratio, particularly among the N-MORB, shows a modest overall decrease toward the east, reaching a minimum value at 112·4°E. Nd isotopic ratios exhibit virtually no along-axis regional gradient east of about 90°E, particularly when the E-MORB data are included.

The two *WW10*-145 glasses and the N-MORB from dredge *WW10*-128 stand out from the main group of data in Fig. 2. All three are characterized by relatively high $^{87}Sr/^{86}Sr$ for their ε_{Nd} values (Fig. 2e), especially the *WW10*-128 (110·41°E) sample, which also has the highest ε_{Nd} (+9·8) of the samples we analyzed. The only higher ε_{Nd} values reported anywhere along the SEIR are for lavas from just west (zone B4) of the boundary between Indian- and Pacific-MORB mantle within the AAD near 126°E (Pyle *et al.*, 1992; Hanan *et al.*, 2000) (Figs 3f and 4a). The two glasses from dredge *WW10*-145 have by far the lowest $^{206}Pb/^{204}Pb$ values in our dataset (17·362 and 17·594). Lavas with broadly similar isotopic compositions are present at widely separated locations along the Indian Ocean ridges, particularly in the vicinity of the Indian Ocean triple junction at the western end of the SEIR and on the northern Carlsberg Ridge (Fig. 4b); even lower $^{206}Pb/^{204}Pb$ values (as low as 16·87) are found in the 39–41°E section of the Southwest Indian Ridge.

The $^{3}He/^{4}He$ ratio gradually decreases from 8·5–9·7 R_A at the western end of our study area to 6·4–7·4 R_A

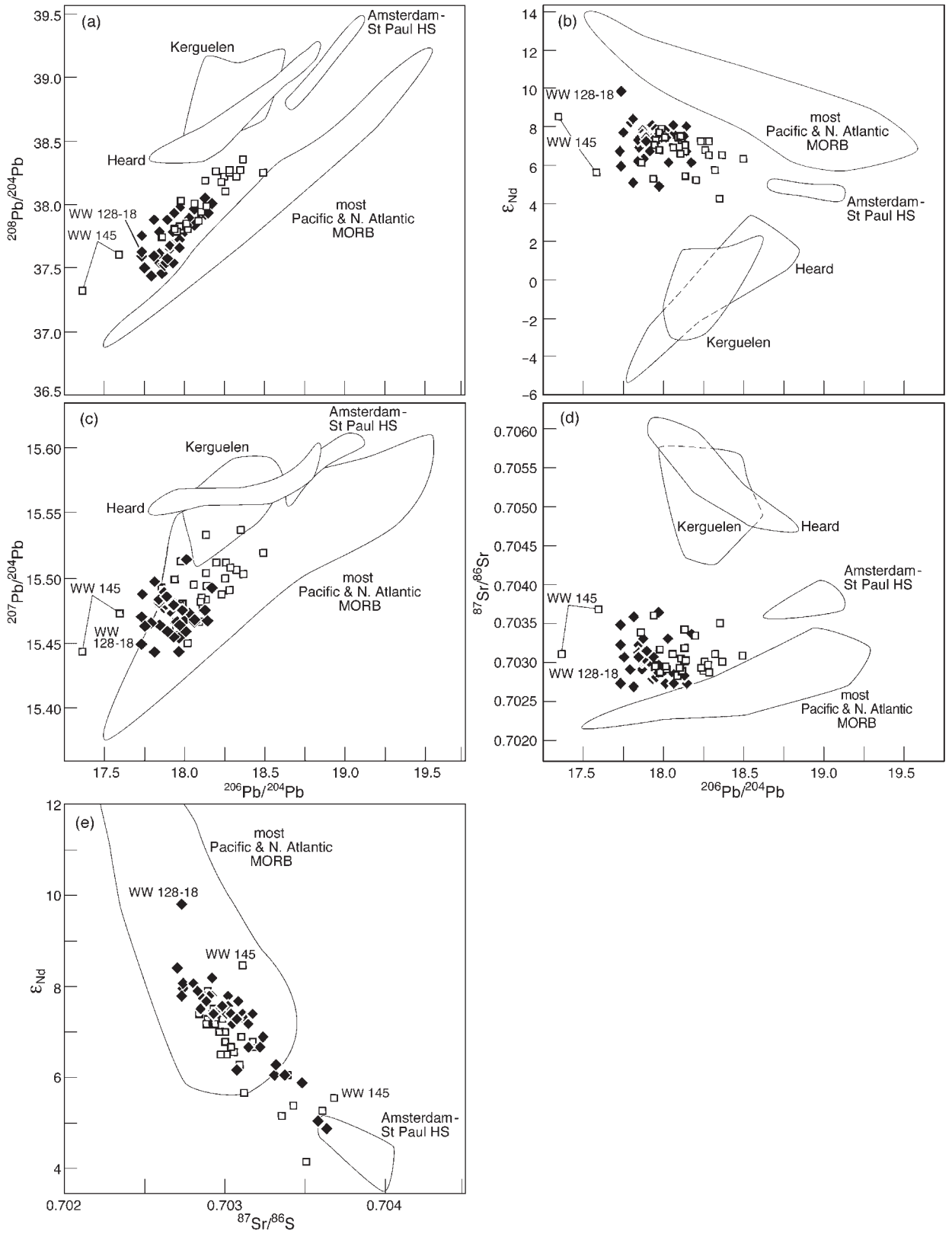
(a)
Amsterdam-St Paul HS
Kerguelen
Heard
most Pacific & N. Atlantic MORB
WW 128-18
WW 145
208Pb/204Pb
(b)
WW 128-18
WW 145
most Pacific & N. Atlantic MORB
Amsterdam-St Paul HS
Heard
Kerguelen
εNd
(c)
Amsterdam-St Paul HS
Kerguelen
Heard
most Pacific & N. Atlantic MORB
WW 145
WW 128-18
207Pb/204Pb
206Pb/204Pb
(d)
Kerguelen
Heard
Amsterdam-St Paul HS
WW 145
WW 128-18
most Pacific & N. Atlantic MORB
87Sr/86Sr
206Pb/204Pb
(e)
most Pacific & N. Atlantic MORB
WW 128-18
WW 145
WW 145
Amsterdam-St Paul HS
εNd
87Sr/86S

at the eastern end (Fig. 3d). All samples with $^{3}He/^{4}He$ >7·7 R_A are from west of 100°E, where the axial depth gradient is slightly shallower and where very few E-MORB were recovered. All but one sample from east of 100°E have $^{3}He/^{4}He$ <7·4 R_A and the majority of those from east of 105°E have $^{3}He/^{4}He$ <7·0 R_A. Farther east, in the AAD, all but the two samples with the highest ε_{Nd} have values between 6·2 and 7·7 R_A (Graham *et al.*, 1990; D. W. Graham, unpublished data, 2000). Worldwide, values below 7·0 are unusual for MORB (e.g. Anderson, 2000); in areas far from high-$^{3}He/^{4}He$ hotspots, MORB generally have $^{3}He/^{4}He$ of 7–9 R_A (e.g. Graham *et al.*, 1999, 2001, and references therein).

With the exception of several samples from the western portion of the study area, there is a weak overall tendency in the 86–118°E data for the highest-Δ8/4, most strongly Indian-MORB-type lavas to have rather low $^{3}He/^{4}He$ (Fig. 5a). However, although the along-axis pattern for He isotopes exhibits a trough that reaches a minimum around 105–109°E, in the same portion of the ridge as the maximum in the broad peak in $^{206}Pb/^{204}Pb$ and $^{208}Pb/^{204}Pb$, He and Pb isotope ratios do not display any simple correlation (Fig. 5b and c). Geographically, samples from west of 100°E constitute a distinctly different He isotope population from those east of 100°E (including the AAD), the two groups producing a V-shaped pattern in Fig. 5a–d. As with He–Pb, no simple correlation between He and Sr or Nd isotopes is present in the 86–118°E dataset overall but, in contrast to Pb, rough He–Sr (Fig. 5d) and He–Nd isotope correlations are seen when only the N-MORB samples are considered (Pearson correlation coefficient $r = 0{\cdot}75$ and $-0{\cdot}63$, respectively). They cannot obviously be explained in terms of binary mixing, however, because the low-$^{3}He/^{4}He$, low-$^{87}Sr/^{86}Sr$ (Fig. 5d), high-ε_{Nd} N-MORB samples, all of which are from east of 100°E, have relatively high $^{208}Pb/^{204}Pb$ and do not lie along a trend with the other N-MORB in Fig. 5b. These observations indicate that much of the mantle west of ~100°E has experienced a different geochemical history from that farther east.

In addition to the large-scale longitudinal variations, an isotopic 'fine structure' is also evident along-axis. As at larger scales, the locations of small-scale excursions from the general regional patterns tend to differ for different isotope ratios. For example, the maximum $^{206}Pb/^{204}Pb$ value observed is in an E-MORB at 95·93°E (see vertical dashed line in Fig. 3); in $^{208}Pb/^{204}Pb$ this location is a local high but not a maximum; in ε_{Nd} it barely stands out, and in Sr isotopes it does not stand out at all. There is a distinct local peak in Δ8/4 but the maximum is at 96·83°E, not 95·93°E; $^{3}He/^{4}He$ also displays a local maximum at 96·83°E, although, as noted above, with the exception of this and several other samples from the western part of the study area, the highest-Δ8/4 lavas tend to have low $^{3}He/^{4}He$. Likewise, a local high occurs in $^{87}Sr/^{86}Sr$ at 97·51°E; the excursion here in ε_{Nd} is less marked, and absent in $^{206}Pb/^{204}Pb$, $^{208}Pb/^{204}Pb$, and He isotope ratios.

A notable exception to this generally poor inter-isotope correspondence is at the western end of the study area (~86–90°E), where a peak is present in all isotope ratios. In detail, however, the shape of this peak varies from one isotope ratio to another and the extreme values again do not all occur at the same location: the peak in Δ8/4 is at 87·09°E, that in $^{206}Pb/^{204}Pb$ and $^{208}Pb/^{204}Pb$ at 89·32°E, and that in $^{3}He/^{4}He$, $^{87}Sr/^{86}Sr$, and ε_{Nd} at 88·04°E.

Relationships of isotopes to physical and chemical characteristics

Neither the general shapes nor the details of the longitudinal isotopic patterns correlate well with physical discontinuities in the ridge axis (the main offsets in the axis are indicated by tick marks at the top of panels in Fig. 3). Thus, with the present sampling, physical segmentation of the ridge in the 86–118°E region appears largely independent of mantle isotopic composition. Moreover, a relatively minor role for along-axis flow and mixing of magma within individual ridge segments is suggested by trends in one or more isotope ratios that continue across segment boundaries (e.g. at 92°E, 106·5°E, 114°E), together with the co-occurrence of E- and N-MORB within individual segments and even within some individual dredge hauls.

The closest oceanic islands to the 86–118°E section of the SEIR are Amsterdam and St. Paul, some 700 km from our westernmost station (Fig. 1). These islands sit atop the Amsterdam–St. Paul Platform, generally believed to be the expression of a near-ridge hotspot (e.g. Graham *et al.*, 1999; Johnson *et al.*, 2000). The next

Fig. 2. Pb, Nd and Sr isotopic data for the 86–118°E SEIR glasses. ◆, N-MORB; □, E-MORB. The field for the Amsterdam–St. Paul hotspot (HS) encompasses the data of Hamelin *et al.* (1986), Michard *et al.* (1986), Dosso *et al.* (1988), Salters & White (1998) and W. M. White (unpublished data, 1995) for the islands of Amsterdam and St. Paul; that for the Kerguelen–Heard hotspot is from the data of Dosso *et al.* (1979), Dosso & Rama Murthy (1980), Storey *et al.* (1988), Gautier *et al.* (1990), Weis *et al.* (1993, 1998), Barling *et al.* (1994) and Yang *et al.* (1998) and excludes Kerguelen basalts thought to have a component of MORB-type material in their source (see Yang *et al.*, 1998), and evolved plutonic rocks. The Pacific and North (N.) Atlantic MORB field encompasses >95% of published high-quality data; sources are those listed by Mahoney *et al.* (1998), plus data and additional references of Castillo *et al.* (1998, 2000), Dosso *et al.* (1999), Schilling *et al.* (1999), Sturm *et al.* (1999) and Vlastélic *et al.* (2000).

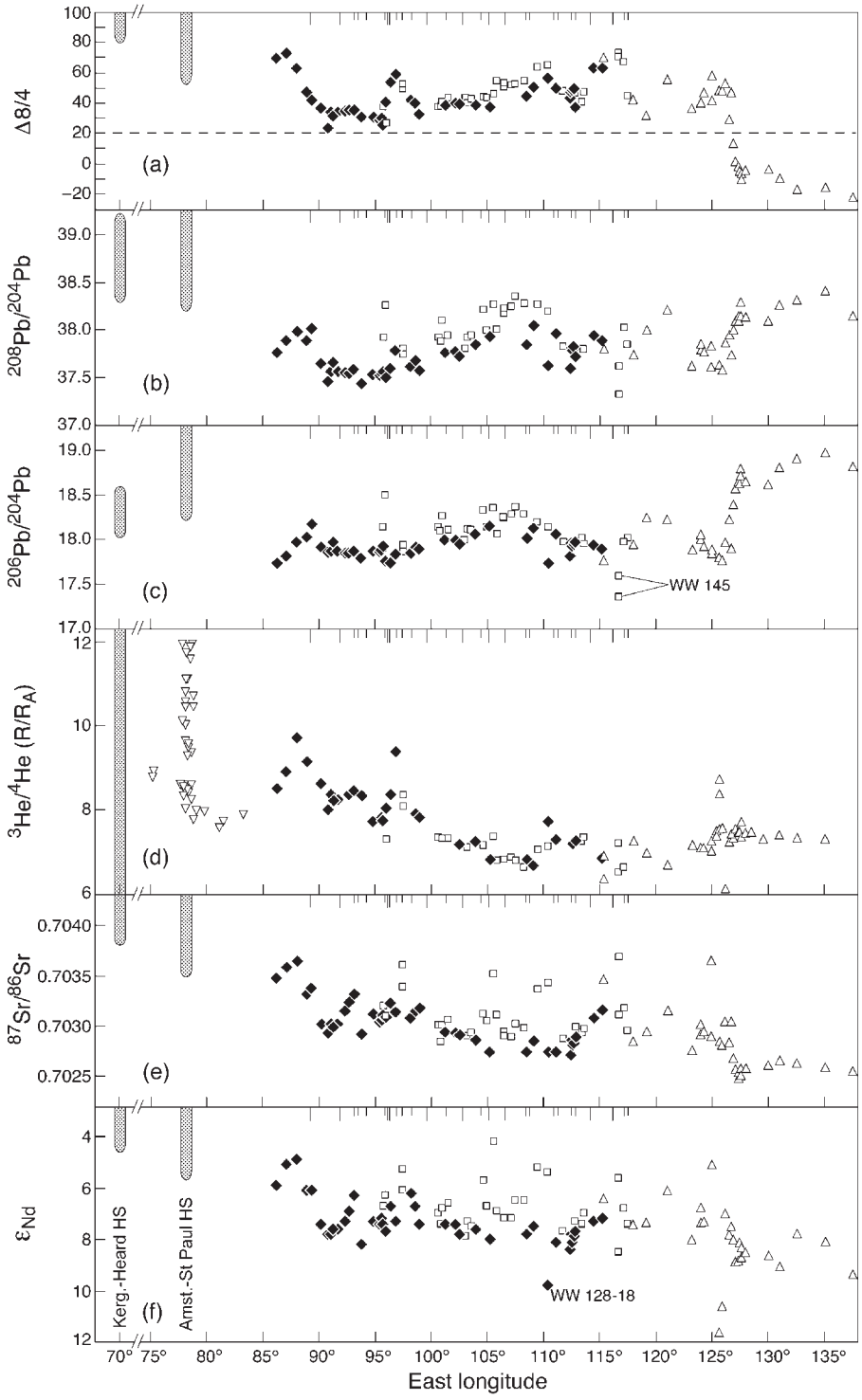

Fig. 3. Longitudinal patterns of SEIR isotopic data. ◆, 86–118°E N-MORB; □, E-MORB glasses. △, data for the AAD area (Klein *et al.*, 1988; Graham *et al.*, 1990; Pyle *et al.*, 1992; D. W. Graham, unpublished data, 2000). ▽, He-isotope data for the SEIR west of 86°E to just west of the Amsterdam–St. Paul hotspot (Graham *et al.*, 1999). Gray fields for the Kerguelen–Heard and Amsterdam–St. Paul hotspots (HS) are from sources listed for Fig. 2, plus Hilton *et al.* (1995), Valbracht *et al.* (1996) and Nicolaysen *et al.* (1998, and in preparation). Dashed line at $\Delta 8/4 = 20$ in (a) separates nearly all Pacific and Indian MORB. Dashed vertical line at 95·93°E marks the location of maximum $^{206}Pb/^{204}Pb$ (see text). The tick marks at the top of each panel indicate the principal first-order (longer marks) and second-order (shorter marks) physical offsets in the 86–118°E portion of the ridge (Cochran *et al.*, 1997; Sempéré *et al.*, 1997). Note that ε_{Nd} scale is reversed in (f).

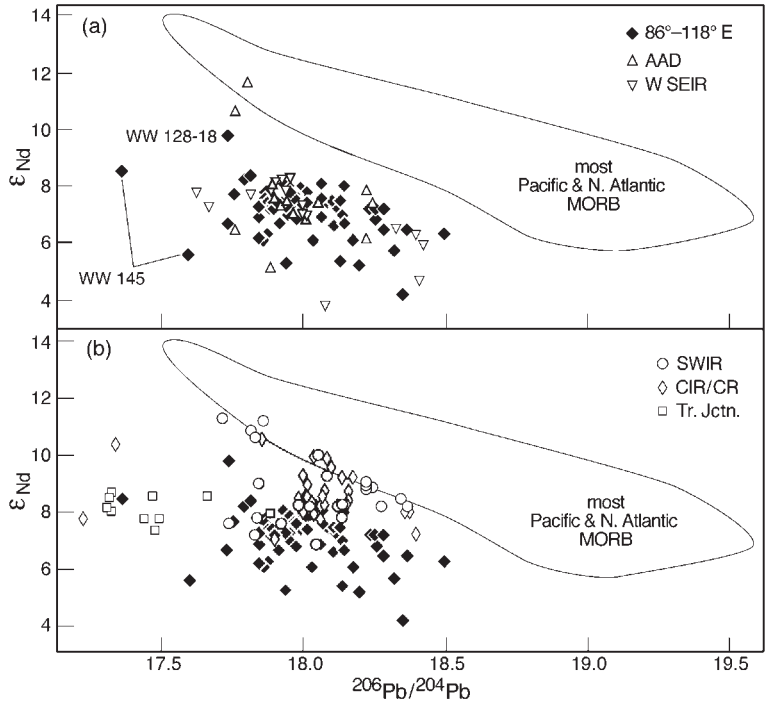

Fig. 4. ε_{Nd} vs $^{206}Pb/^{204}Pb$, comparing results for the 86–118°E SEIR (◆, both N- and E-MORB) with data for other parts of the Indian Ocean ridge system. Data for sections of ridges near hotspots are not included (e.g. the 39–41°E section of the Southwest Indian Ridge and the SEIR near Amsterdam–St. Paul). (a) Comparison with the Indian-MORB-type portion of the AAD and the western 700 km of the SEIR (Hamelin *et al.*, 1986; Michard *et al.*, 1986; Dosso *et al.*, 1988; Klein *et al.*, 1988; Pyle *et al.*, 1992); the two data points with markedly high ε_{Nd} are from the easternmost part of the Indian-MORB-type portion of the AAD, between 125°E and 126°E. (b) Comparison with western Indian Ocean ridges: the Southwest Indian Ridge (SWIR) east of 26°E, the Central Indian and Carlsberg ridges (CIR/CR), and the Indian Ocean triple junction (Tr. Jctn.) (Hamelin & Allègre, 1985; Price *et al.*, 1986; Ito *et al.*, 1987; Mahoney *et al.*, 1989, 1992; J. J. Mahoney, unpublished data, 2000; Rehkämper & Hofmann, 1997).

closest islands are the Kerguelen group and Heard and McDonald, which are built upon the older lithosphere of the Kerguelen Plateau. Although there has been some speculation that two hotspots might lie beneath the plateau, as the Kerguelen group is located nearly 300 km from Heard and nearby McDonald and is isotopically rather distinct from them, all are commonly attributed to a single hotspot (e.g. Weis *et al.*, 2002) situated some 1600 km to the SW of our westernmost dredge sites (Fig. 1). Yet, unlike some hotspot-free ridge sections along which isotopic parameters bear little relationship to axial depth or major or trace element composition, such as parts of the East Pacific Rise (e.g. Bach *et al.*, 1994; Mahoney *et al.*, 1994), some correlations are present at 86–118°E that are superficially similar to some of those seen on ridges located much closer to hotspots (e.g. Verma *et al.*, 1983; Schilling *et al.*, 1999). In particular, $^{3}He/^{4}He$ (Graham *et al.*, 2001) and Δ8/4 exhibit rough correlations with axial depth and/or fractionation-adjusted Na- or Fe-oxide contents (see Fig. 6a–d). On the other hand, ε_{Nd}, $^{206}Pb/^{204}Pb$, and $^{87}Sr/^{86}Sr$ do not. Many incompatible element ratios also show a crude covariation with fractionation-adjusted Na or Fe (Fig. 6e and f).

Pb, Nd and Sr isotopes do correlate roughly with many incompatible element ratios, including ratios involving elements that possess significantly different bulk partition coefficients (e.g. U/Pb, La/Sm) and those with more similar bulk partition coefficients (e.g. Sm/Nd, Nb/La, Nd/Pb); some examples are shown in Fig. 7. All the correlations observed are poor (e.g. assuming the relationships are linear, $|r|$ is always <0·8 and often much less). Correlations of isotope ratios and their respective parent–daughter element ratios similar to those in Fig. 7a–c and e have been reported recently for the 10–24°N and 38–41°N sections of the Mid-Atlantic Ridge (Dosso *et al.*, 1999). In general, very poor or no correlations exist in our dataset between isotopic ratios and inter-element ratios involving two moderately incompatible elements, particularly those affected strongly by melting in the presence of garnet (e.g. Zr/Y, Hf/Lu; not shown); the same is true for some highly incompatible element pairs (Nb/U, Ba/Th). Helium isotopes display a crudely L-shaped relationship with ratios such as $(La/Sm)_n$ (Fig. 5e); this reflects the fact that, as noted above, the N-MORB are from throughout the study area and encompass nearly the entire range observed in $^{3}He/^{4}He$

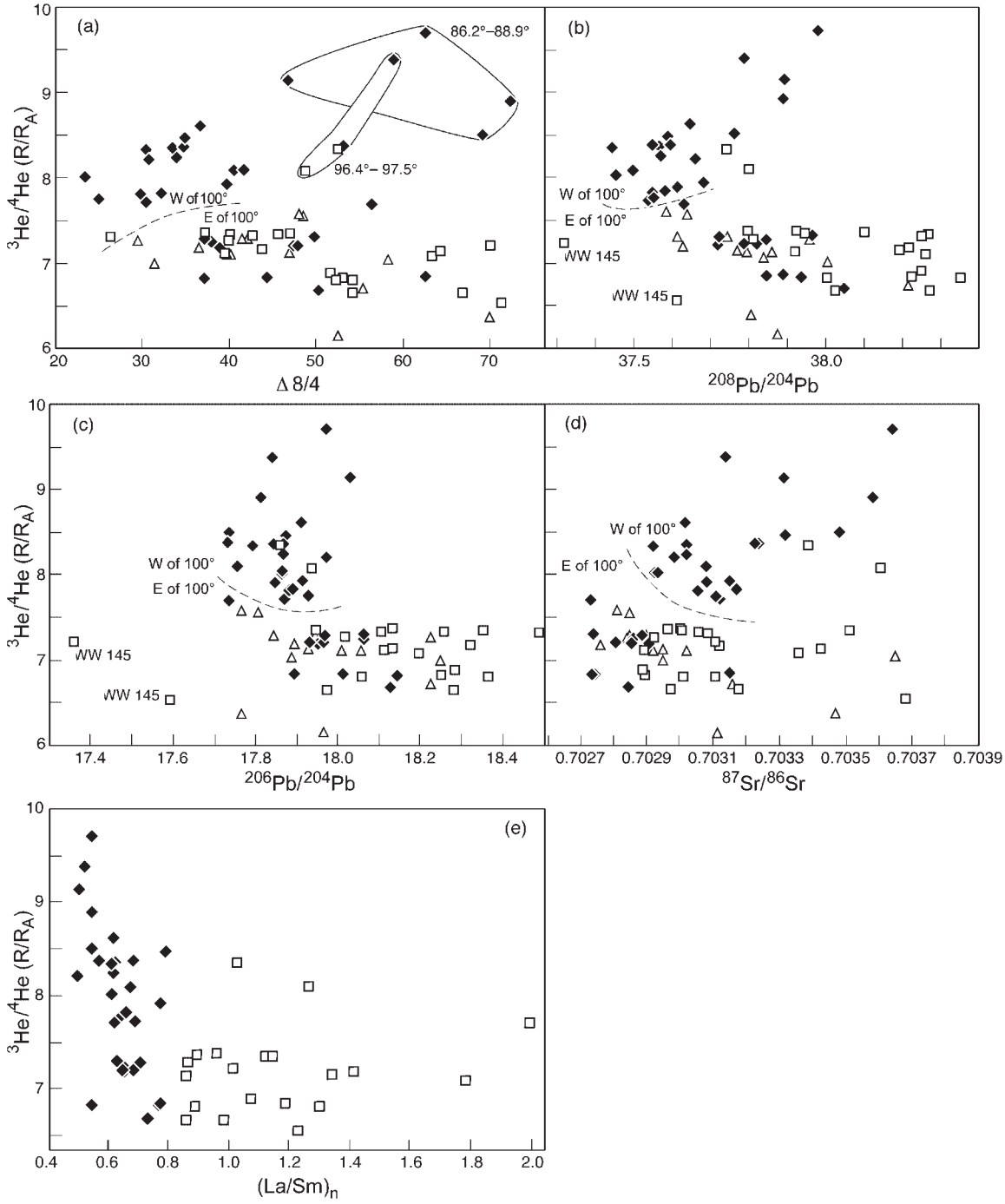

Fig. 5. $^3He/^4He$ (as R/R_A) vs (a) Δ8/4, (b) $^{208}Pb/^{204}Pb$, (c) $^{206}Pb/^{204}Pb$, (d) $^{87}Sr/^{86}Sr$, and (e) $(La/Sm)_n$. ◆, 86–118°E N-MORB data; □, E-MORB. △, AAD data (Klein *et al.*, 1988; Graham *et al.*, 1990, 1999; Pyle *et al.*, 1992, 1995; D. W. Graham, unpublished data, 2000).

whereas almost all of the E-MORB are from the eastern portion of the region, where $^3He/^4He$ values are all rather low. Correlations of element ratios with $^{87}Sr/^{86}Sr$ (of which that with Ba/Nd is one of the best; Fig. 7i) generally are substantially poorer than those with Pb or Nd isotopes, and the overall correlation between $^{87}Sr/^{86}Sr$ and Rb/Sr is essentially nonexistent (Fig. 7e). This is not just an effect of variable plagioclase fractionation on Rb/Sr (Sr being a compatible element in feldspar), because Rb/Sr correlates better with Pb and Nd isotopes than with $^{87}Sr/^{86}Sr$ (e.g. Fig. 7f). However, if samples from west of 100°E (circles in Fig. 7e and i) are excluded,

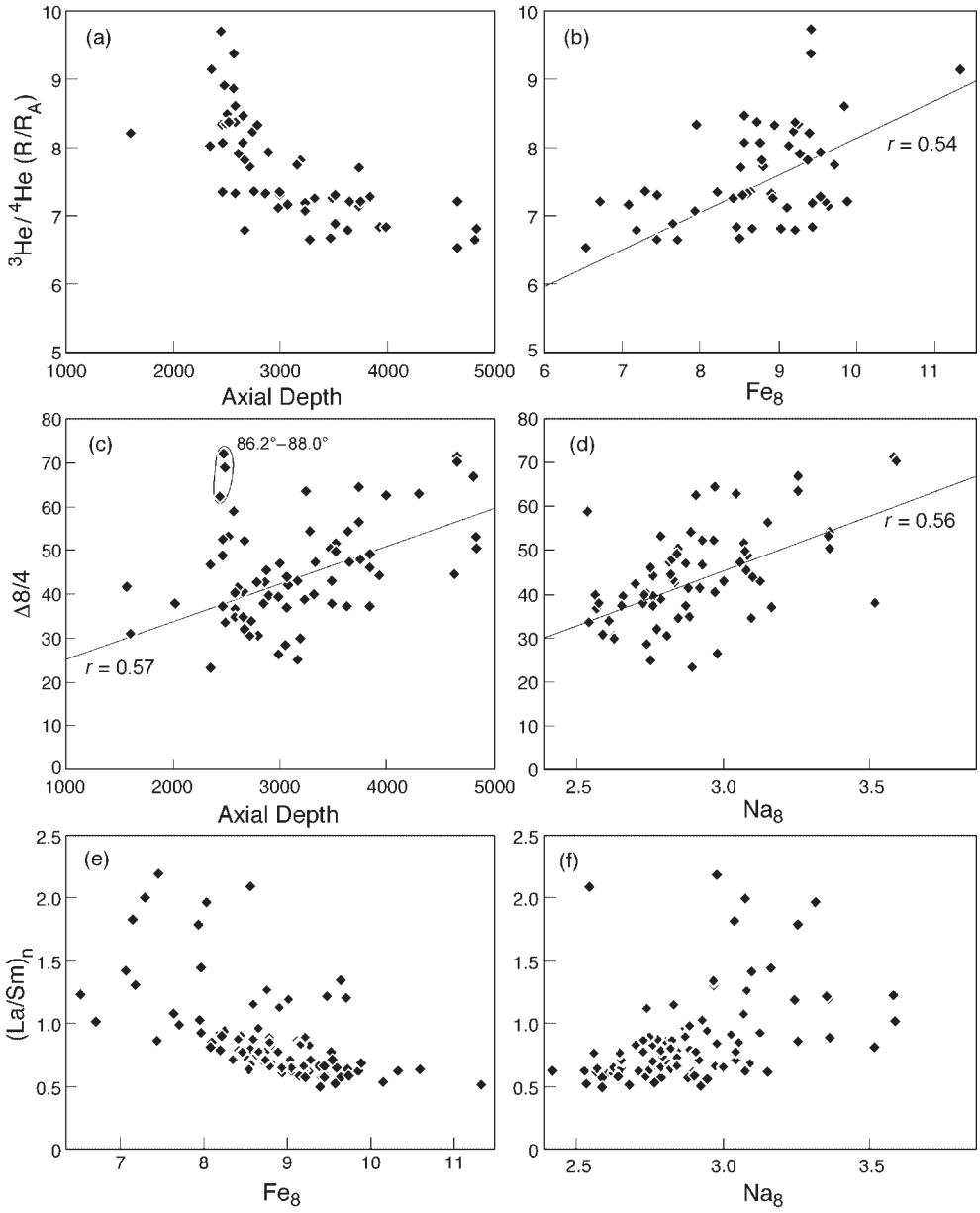

Fig. 6. Variation of $^3He/^4He$ with axial depth (a) and Fe_8 (b), of $\Delta 8/4$ with axial depth (c) and Na_8 (d), and of $(La/Sm)_n$ with Fe_8 (e) and Na_8 (f) for 86–118°E SEIR glasses (◆, both N- and E-MORB). Fe_8 and Na_8 are Fe- and Na-oxide weight percentages adjusted for fractionation to estimated values at 8 wt % MgO (see Klein & Langmuir, 1987). Regression lines in (b)–(d) are robust fits with errors in x and y (e.g. Rousseeuw & Leroy, 1987); r is the correlation coefficient. Regression in (c) excludes three glasses from the western end of the study area (86·2°–88·0°).

$^{87}Sr/^{86}Sr$ and Rb/Sr correlate weakly (r = 0·59), and other correlations involving $^{87}Sr/^{86}Sr$ improve (e.g. that with Ba/Nd to r = 0·81).

DISCUSSION

Mantle flow and role of hotspot mantle

Although their total isotopic range is substantial, all SEIR samples from west of the AAD possess unequivocally Indian-MORB-type isotopic signatures (e.g. Fig. 3a). Thus, the isotopic boundary at 126°E marks the westernmost extent of Pacific-type MORB along the SEIR. No evidence exists to suggest that mantle convection west of 126°E is stirring Pacific- and Indian-MORB-source mantle together in stringers much larger than the scale of sampling (~35 km), as would be indicated by along-axis interdigitation of the two types of basalts. Nor is there any evidence that the two types of mantle are variably mixing at scales similar to or smaller than the

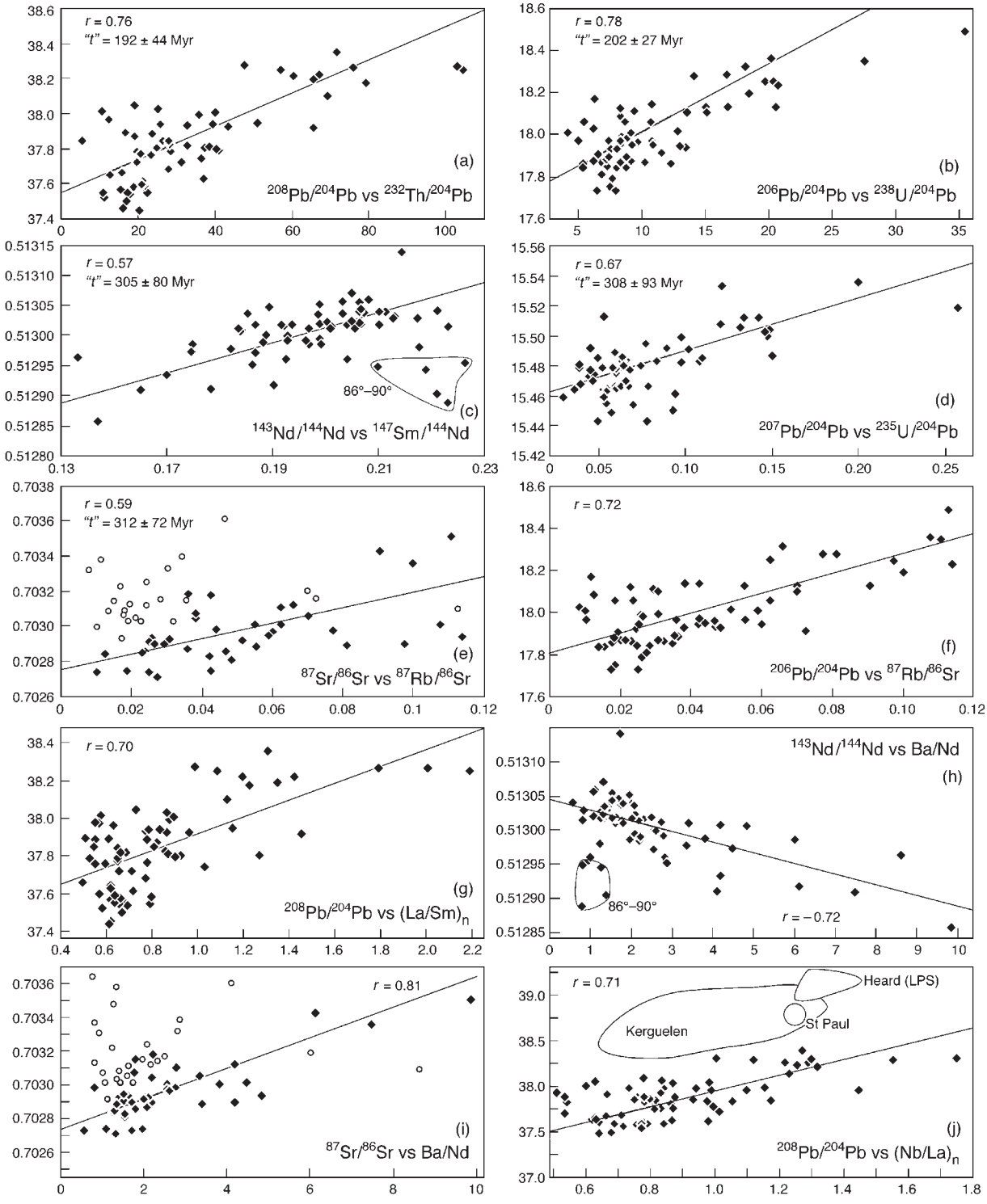

Fig. 7. Variations of Pb, Nd, and Sr isotopes with incompatible element ratios. In the label inside each panel, the first ratio is for the *y*-axis and the second the *x*-axis label (i.e. *y* vs *x*). The regression lines are robust fits with errors in *x* and *y*. ◆, data for both N- and E-MORB, except in (e) and (i), where data for samples from west of 100°E are indicated by ○. The regression lines in (e) and (i) apply only to samples from east of 100°E (i.e. ◆). Data for the two low-$^{206}Pb/^{204}Pb$ samples from dredge *WW10*-145 and for the 86–90°E samples are not used in the regressions. Fields in (j) for the island volcanoes are from data of Dosso *et al.* (1988), Storey *et al.* (1988), Gautier *et al.* (1990), Weis *et al.* (1993, 1998), Barling *et al.* (1994), Yang *et al.* (1998) and J. J. Mahoney (unpublished data, 2000). LPS, Laurens Peninsula Series. The parent–daughter nuclide ratios in (a)–(f) have been calculated from measured Rb/Sr, Sm/Nd, U/Pb, and Th/Pb concentration ratios.

scale of sampling, as the presence of isotopic gradients and intermediate compositions between Indian and Pacific MORB types would indicate.

Nevertheless, the broad along-axis gradients in several of the isotopic patterns in the 86–118°E region (Fig. 3) may reflect some type of large-scale mantle flow and mixing. However, contrary to predictions based upon the regional eastward decrease in asthenospheric temperature (Marks *et al.*, 1991; Sempéré *et al.*, 1997; West *et al.*, 1997), a major eastward flow of hotspot mantle from either the Amsterdam–St. Paul or Kerguelen–Heard hotspot is *not* supported by our combined isotopic data. Going eastward, the 'baseline' $^{87}Sr/^{86}Sr$ value decreases slightly to as far east as 112·4°E, a trend that appears consistent with eastward flow and gradual mixing of high-$^{87}Sr/^{86}Sr$ hotspot-derived mantle into relatively low-$^{87}Sr/^{86}Sr$, ambient MORB-type mantle. However, the along-axis variations in Pb isotope ratios are not consistent with such an interpretation. Both hotspots have high $^{208}Pb/^{204}Pb$, yet $^{208}Pb/^{204}Pb$ shows a broad eastward increase over much of the region, from 90°E to 107·5°E, just the opposite of the trend expected if high-$^{208}Pb/^{204}Pb$ mantle emanating from either hotspot were flowing east and mixing with normal MORB-type mantle. The same is true for $^{206}Pb/^{204}Pb$, particularly for Amsterdam–St. Paul hotspot mantle. Likewise, both hotspots have high Δ8/4, yet over most of the study area, from about 90°E to 117°E, Δ8/4 exhibits an overall increase to the east rather than the west. Also, although both hotspots have low ε_{Nd}, particularly the Kerguelen–Heard hotspot, almost no large-scale gradient in ε_{Nd} is present east of about 90°E.

Moreover, the along-axis isotopic variations cannot obviously be explained by appealing to long-term temporal changes in hotspot mantle composition; that is, that the SEIR in the 86–118°E region taps ancient hotspot-derived mantle that is isotopically different from recent hotspot mantle. Cretaceous and Early Tertiary lavas of the Kerguelen Plateau and Broken Ridge (products of the ancestral Kerguelen–Heard hotspot; e.g. Duncan & Storey, 1992) and the Ninetyeast Ridge (produced by the Kerguelen–Heard hotspot and perhaps partly by the Amsterdam–St. Paul hotspot; e.g. Luyendyk & Rennick, 1977; Duncan & Storey, 1992) encompass a wider range of isotopic variation than recent ones (e.g. Davies *et al.*, 1989; Weis *et al.*, 1989; Saunders *et al.*, 1991; Salters *et al.*, 1992; Mahoney *et al.*, 1995; Frey *et al.*, 2002; Ingle *et al.*, 2002; Neal *et al.*, 2002). However, like the younger lavas, the Cretaceous and Early Tertiary lavas lack the combination of features required of any hotspot end-member that would account for the 86–118°E isotopic patterns. For example, the old hotspot lavas do not have high Δ8/4 together with relatively low $^{87}Sr/^{86}Sr$ (as would be required of one end-member for much of the eastern part of the study area) or vice versa (as for much of the 90–100°E portion).

He isotopes may at first seem to offer support for a general eastward flow (and aging and/or dilution) of hotspot mantle. SEIR lavas near the Amsterdam–St. Paul hotspot reach much higher $^{3}He/^{4}He$ (to 14·1 R_A; Graham *et al.*, 1999) than the 86–118°E or AAD lavas and, east of 88·0°E, $^{3}He/^{4}He$ shows an overall eastward decrease. The He isotopic ratios of Kerguelen–Heard lavas are widely variable, with $^{3}He/^{4}He$ ranging as high as 18 R_A; the higher values are presumed to reflect a high-$^{3}He/^{4}He$ hotspot mantle source (the lower values may result from variable interaction of hotspot magmas with the relatively old, thick Kerguelen Plateau lithosphere on which these volcanoes sit) (Hilton *et al.*, 1995; Valbracht *et al.*, 1996; Nicolaysen *et al.*, 1998). However, along the SEIR, $^{3}He/^{4}He$ not only decreases to the east of 88°E but also decreases to values as low as 7·6 to the west of 88°E (Fig. 3d), a feature difficult to explain by a regional eastward flow of mantle from hotspots far to the west of our study area. Indeed, Graham *et al.* (1999) concluded that asthenosphere in the vicinity of the Amsterdam–St. Paul hotspot is at present flowing mostly to the NNE.

Rather than emanating from a hotspot in a relatively steady flux, hotspot-derived material conceivably might enter a general eastward mantle flow only periodically, in pulses separated by millions of years, eventually producing relatively complicated along-axis isotopic patterns that would contain more than one peak. In the $^{206}Pb/^{204}Pb$ pattern, for example, the broad peak at 107·5°E, the peak at 89·3°E, and possibly that at 95·9°E (Fig. 3c) could correspond to three such pulses. As noted above, however, peaks in one or more of the other isotope ratios fail to coincide geographically—or necessarily even in number—with those in $^{206}Pb/^{204}Pb$. Nor are the locations of the peaks or troughs in one isotopic ratio shifted consistently to the west or east relative to those of other isotopic ratios [along-axis shifts in a consistent direction above shallow east-flowing mantle might be explicable as an effect of differential partitioning of the different elements in the melting region or, for He, just below it (Graham *et al.*, 1992; Poreda *et al.*, 1993; Mahoney *et al.*, 1994; Schilling *et al.*, 1999)]. For example, the westernmost peak in $^{3}He/^{4}He$ lies slightly west of that in $^{206}Pb/^{204}Pb$ but the easternmost He isotope peak is well to the east of that in $^{206}Pb/^{204}Pb$. Although an eastward component of asthenospheric flow seems inevitable, given the bathymetric and thermal gradients across the 86–118°E region (Marks *et al.*, 1991; Cochran *et al.*, 1997; Sempéré *et al.*, 1997; West *et al.*, 1997) and the probable long-term eastward relative motion of the asthenosphere (Doglioni, 1990; Ricard *et al.*, 1991; Smith & Lewis, 1999), we conclude that hotspot-derived mantle with either Amsterdam–St. Paul or Kerguelen–Heard compositions cannot be a dominant constituent of such flow.

Regardless of the nature of mantle flow and mixing, is mantle derived from either of these hotspots involved at all in generating MORB in the study area? Mixing of sufficient amounts of isotopically distinct hotspot-type mantle into moderately heterogeneous normal MORB-type mantle should produce isotopic arrays in Fig. 2 that point approximately toward the hotspot end-member's composition. Fields for Kerguelen and Heard islands cover a wide isotopic range but are easily distinguished from the Amsterdam–St. Paul hotspot field (as represented by the volcanoes of St. Paul and Amsterdam islands), although the high-$^{206}Pb/^{204}Pb$ ends of the Kerguelen and Heard fields approach the compositions seen at Amsterdam and St. Paul. Data for small subsections of the 86–118°E SEIR do not form well-defined arrays pointing to one hotspot field or the other in all isotope diagrams. Arrays defined by larger subsections, and by the 86–118°E dataset as a whole, are broad (and thus could potentially record some influence by both types of hotspot mantle), but the longest dimension of the arrays in Fig. 2a–c is oriented roughly toward the Amsterdam–St. Paul field rather than the low-$^{206}Pb/^{204}Pb$ ends of the Kerguelen or Heard fields. As a group, therefore, the 86–118°E isotopic data appear to allow at least a modest role for Amsterdam–St. Paul-type or possibly high-$^{206}Pb/^{204}Pb$ Heard-Island-type mantle, while permitting only a small influence, if any, of Kerguelen–Heard-type material having $^{206}Pb/^{204}Pb$ at the low end of the range observed for these islands (indeed, rather than representing hotspot mantle signatures, the Kerguelen and Heard lavas with the lowest $^{206}Pb/^{204}Pb$ may be contaminated by old continental material present in the lithosphere of the Kerguelen Plateau; Weis *et al.*, 2002).

Additional insight is provided by an evaluation of incompatible element ratios; specifically, whether they are consistent with mixing between hotspot mantle and typical, moderately heterogeneous MORB-type mantle. In general, hotspot-type mantle will have relative enrichments in the highly incompatible elements compared with MORB-source mantle. Only a few combined isotopic and trace element data have been published for the moderately evolved lavas making up the islands of Amsterdam and St. Paul; many more data exist for the Kerguelen Archipelago and Heard Island, but most are for lavas considerably more alkalic (basalts, basanites, nephelinites, and phonolites) than the tholeiitic basalts erupted along the SEIR, and probably represent rather small fractions of partial melting (e.g. Barling *et al.*, 1994; Weis *et al.*, 1998). Also, in some of the island samples, abundances of mobile elements such as Rb, K, and possibly Ba may have been modified by subaerial weathering. Hence, not all of the measured incompatible element ratios in the island lavas are close to the values in their mantle sources. However, ratios of alteration-resistant, highly incompatible elements with closely similar bulk distribution coefficients, such as Nb and La, should not be changed much by either moderate amounts of alteration or even rather small amounts of partial melting [Nb tends to be slightly more incompatible than La (e.g. Niu & Batiza, 1997), so small-degree melts may have slightly higher Nb/La than their sources]. Figure 7j shows that the available data for both St. Paul and Kerguelen–Heard lavas have markedly lower Nb/La than required to explain the 86–118°E SEIR trend; that is, they do not lie along either a linear or hyperbolic extension of it. More trace element data are needed for Amsterdam–St. Paul hotspot lavas before any conclusive statement can be made, but the existing results provide no evidence that material derived from either hotspot plays more than a minor role in the 86–118°E SEIR source mantle. [As an aside, we also note that anciently subducted, recycled marine sedimentary material, whether supplied by hotspots or not, appears not to be a suitable mixing end-member for producing the elongate SEIR array, because such material would be characterized by high $^{208}Pb/^{204}Pb$ yet low, not high, Nb/La values (probably $\sim$0·3, on average; e.g. Rehkämper & Hofmann, 1997)].

The one place in the entire region where isotopic variations appear broadly consistent with the presence of a moderate amount of hotspot-derived mantle is at the western end of the study area, at $\sim$86–90°E (Fig. 3). Intriguingly, this is close to the location where, on the basis of satellite-derived gravity data, Small & Sandwell (1994) and Small (1995) proposed that an asthenospheric jet or channel some 1600 km long may carry mantle from the Kerguelen–Heard hotspot to the SEIR. However, according to the plume source–ridge sink model (Schilling, 1985), in which a residual connection remains between a hotspot and a spreading ridge after the ridge has overridden the hotspot, the predicted width of an axial geochemical anomaly 1600 km from a hotspot would be much smaller (<50 km) than the isotopic peak at 86–90°E. The geochemical evidence for a Kerguelen–Heard hotspot influence is weak, for samples from the western part of the study area do not define arrays that consistently point toward Kerguelen–Heard isotopic or isotope–element ratio space, and all of the samples from west of 95·8°E are incompatible-element-depleted N-MORB. In any case, if a flow channel from the Kerguelen–Heard hotspot does exist, our data indicate that its along-axis isotopic signal to the east has disappeared to 'background' values by about 90°E (Fig. 3).

Alternatively, Graham *et al.* (2001) recently suggested that the asthenosphere between St. Paul and the AAD may be vertically zoned, and that the local highs in $^{3}He/^{4}He$ along the SEIR, such as that at 88·0°E, may mark sites where comparatively deep mantle with relatively

high $^{3}He/^{4}He$ is being tapped. Information on the relative depths and amounts of mantle melting is provided by the depth of the ridge axis and fractionation-adjusted major-element characteristics such as glass-group average Fe- and Na-oxide (with lower Fe corresponding to lower mean pressures and higher Na to smaller mean fractions of partial melting) (e.g. Klein & Langmuir, 1987). Rough correlations of the He isotope ratio with these parameters suggest that portions of SEIR mantle melting at relatively shallow depths tend to have lower $^{3}He/^{4}He$ values [Fig. 6a and b, and Graham *et al.* (2001)]. A weak tendency also is evident for the highest-$\Delta 8/4$, most strongly Indian-MORB-type mantle to be associated with greater axial depths and lower amounts of partial melting (Fig. 6c and d) and, by implication, with relatively fusible mantle and perhaps a shallower mean depth of melting. Thus, the rough correlations in Fig. 6 are consistent with at least modest vertical compositional zoning of the sub-ridge mantle. However, the rather poor correspondence of the along-axis He isotope peaks to the peaks in other isotopic ratios (see above) would appear to require that if deeper, higher-$^{3}He/^{4}He$ mantle is welling up in places, it and the shallower asthenosphere it invades must be heterogeneous from one place to another in Sr, Nd, and Pb isotopes.

Mantle isochrons?

Instead of variable mixing between an incompatible-element-depleted MORB mantle end-member and mantle derived from extant hotspots in the eastern Indian Ocean, mixing involving such an end-member and relatively high-$^{206}Pb/^{204}Pb$, incompatible-element-enriched material similar to the 'C' component proposed by Hanan & Graham (1996) to variably affect MORB worldwide may be invoked to account for the elongation of the arrays in Figs 2 and 7. C-type compositions are assumed to represent old recycled oceanic lithosphere, probably delivered to the MORB source mantle over time by multiple mantle plumes. Similarly, involvement of 'low-6/4' or 'EM1'-like, ultimately continentally derived, material with low $^{206}Pb/^{204}Pb$ and ε_{Nd}, and relatively high $^{87}Sr/^{86}Sr$, $^{208}Pb/^{204}Pb$, and $^{207}Pb/^{204}Pb$ may partly explain the breadth of the SEIR arrays in Figs 2 and 7, particularly for the samples from west of 100°E. Unfortunately, such a mixing hypothesis is very difficult to test because it is so general, but would be strengthened if other potential explanations for the 86–118°E data could be ruled out.

Rather than mixing, a possible alternative explanation for the observed relationships among isotopes and between isotopic and incompatible element ratios is that they preserve a record of ancient fractionation (melt enrichment or depletion) in the mantle now feeding the SEIR. If so, the rough correlations between isotopic ratios and their respective parent–daughter element ratios (Fig. 7a–e) could have broad age significance (e.g. Brooks *et al.*, 1976). If these correlations are interpreted as mantle 'errorchrons', then ages calculated from the slopes of lines fitted through the data vary from about 200 to 300 Ma. Although the uncertainty on each of these 'ages' is very large, the values increase in the order ^{232}Th–$^{208}Pb \sim {}^{238}U$–$^{206}Pb < {}^{147}Sm$–$^{143}Nd \sim {}^{235}U$–^{207}Pb. As noted above, no significant $^{87}Sr/^{86}Sr$–$^{87}Rb/^{86}Sr$ correlation is present if all the data are included; but if the samples from the western part of the study area are excluded, a Rb–Sr 'age' similar to that for Sm–Nd and ^{235}U–^{207}Pb is obtained.

Qualitatively, the differences among the three Pb-isotope 'ages' are reminiscent of those commonly seen in systems that, after a period of closed-system decay and ingrowth, have experienced relatively recent open-system modification of parent–daughter ratios. The analogy in the SEIR case presumably would be the modification of mantle U/Pb and Th/Pb ratios by melting and crystallization during sub-ridge magma production and differentiation, with Pb behaving as a less incompatible element than Th or U. More generally, the changes in parent–daughter ratios caused by magma genesis will tend to rotate and degrade any pre-existing isochronal relationships. That the Sm–Nd and Rb–Sr 'ages' are near the older end of the range of those for Pb isotopes is consistent with the relative fractionation (during recent melting and magma formation) of Sm/Nd and Rb/Sr being less than for U/Pb or Th/Pb. Assuming the ages implied by Fig. 7a–e correspond to a single event, the considerable scatter in the correlations (and ages) would reflect (1) differences in bulk distribution coefficients among the different parent–daughter pairs, (2) variations in melt fraction and magmatic differentiation, plus (3) intrinsic isotopic and elemental heterogeneity in the mantle source (see Dosso *et al.*, 1999) not removed by and/or unrelated to any single past enrichment or depletion event or to the recent magmatism producing the SEIR basalts. An additional important factor for $^{207}Pb/^{204}Pb$, in particular, is the comparatively great analytical uncertainty ($\pm 0{\cdot}010$) relative to the observed total range of variation in this ratio (0·093). Substantial intrinsic source heterogeneity in fact appears to be required by (1) the sizeable isotopic ranges present at low values of Th/Pb, U/Pb, and Rb/Sr, (2) the lack of any meaningful correlation between $^{87}Rb/^{86}Sr$ and $^{87}Sr/^{86}Sr$ when the data for samples from the western part of the study area are included and, for example, (3) the low-$^{206}Pb/^{204}Pb$ *WW10*-145 samples and the 86–90°E samples, which fall off many of the correlations defined by the majority of samples. Furthermore, (4) within some individual dredge hauls the isotopic differences between samples, such as the 4·4 ε_{Nd} unit difference between *WW10*-128-1 and -18, are much larger than can be accounted for solely

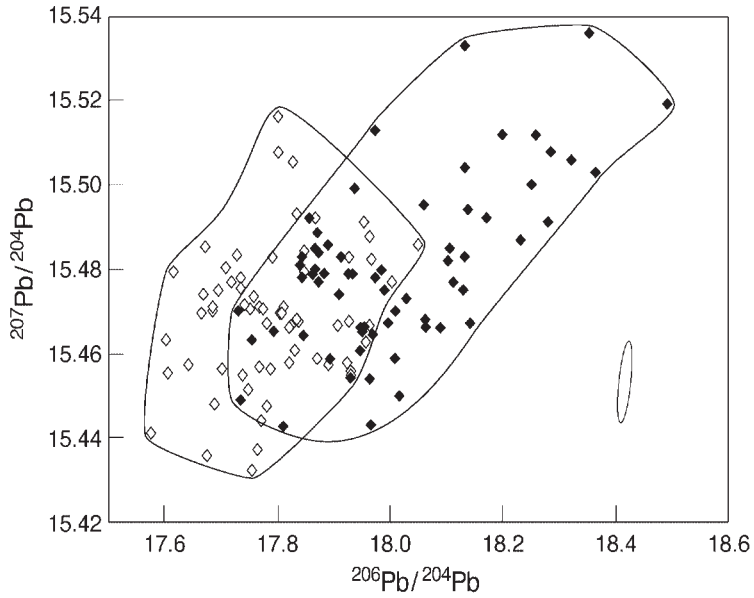

Fig. 8. Hypothetical example of Pb-isotope change that might occur in the source in 250 Myr. ◆, measured values for the 86–118°E glasses; ◇, mantle-source values 250 Myr ago, calculated assuming the U/Pb ratio in the source is half the value measured in the lava. Data for the two *WW10*-145 samples are not shown. Error ellipse is for measured values.

by radiogenic ingrowth in 200–300 Myr with the measured—or any plausible—parent–daughter ratios.

A poorly defined ^{207}Pb–^{206}Pb 'age' of 815 ± 245 Ma can be derived from the slope of the data array in Fig. 2c ($r = 0{\cdot}56$). This value, although significantly greater than the 200–300 Ma values estimated from the correlations in Fig. 7a–e, is less than the 1–2·5 Ga ^{207}Pb–^{206}Pb 'ages' found for many MORB datasets (e.g. Church & Tatsumoto, 1975; Sun, 1980; Galer, 1999), which, at large spatial scales, are commonly interpreted to represent an integrated or mean evolution age of source mantle that has experienced a fairly complicated open-system, several-billion-year history (e.g. White, 1993; but see also Albarède, 2001). In the 86–118°E SEIR mantle source, any 200–300 Ma fractionation event consistent with the correlations in Fig. 7a–e would probably modify preexisting $^{207}Pb/^{204}Pb$–$^{206}Pb/^{204}Pb$ relationships only rather modestly because, as just noted, such an event would only partially eradicate preexisting isotopic heterogeneity. As an illustration, Fig. 8 shows estimated 250 Ma source values, calculated assuming the source U/Pb ratios are half those measured in the respective SEIR lavas [i.e. assuming, simplistically, that recent magmatism has in all cases produced lavas with twice their source's U/Pb value (see White, 1993; Dosso *et al.*, 1999)]. The estimated 250 Ma source field is substantially smaller than the present-day field (mainly in its range of $^{206}Pb/^{204}Pb$) but still sizeable.

Assuming the correlations in Fig. 7a–e do have age significance, we note that the inferred ages bracket the long period of continental stretching and rifting that preceded breakup in East Gondwana, which was followed by fully developed seafloor spreading ~160–170 Myr ago along the paleo-Southwest Indian Ridge (e.g. Coffin & Rabinowitz, 1988; Lawver & Gahagan, 1993). Therefore, one possibility is that the mantle now beneath the SEIR at 86–118°E may preserve a record of small amounts of asthenospheric melting and mantle veining associated with decompression via extension of the overlying lithosphere when this mantle was located beneath the East African–Madagascan–Antarctic region of Gondwana some 200–300 Myr ago. In this context, we note that MORB of the western Southwest Indian Ridge also define a rough ~200 Ma Sm–Nd errorchron (le Roex *et al.*, 1983), and that broadly similar values are indicated by available Sm–Nd isotopic data for the Central Indian, Carlsberg, and central–eastern Southwest Indian ridges (excluding segments nearest the Marion and Réunion hotspots) (Mahoney *et al.*, 1989, 1992; Rehkämper & Hofmann, 1997). (Whether Pb and Sr isotope systematics for these ridges yield similar results is unclear because many of the analyzed samples are not glasses but crystalline basalts affected by variable amounts of seawater alteration, and few U and Th abundance data are as yet available.)

On the other hand, errorchrons in this same general age range also have been observed for ridges far outside the Indian Ocean. The most recent and well-documented example is the correlation of $^{206}Pb/^{204}Pb$, $^{208}Pb/^{204}Pb$, and Nd and Sr isotopes with their respective parent–daughter

ratios reported by Dosso *et al.* (1999) for the 10–24°N and 38–41°N sections of the Mid-Atlantic Ridge. The corresponding ages overlap those inferred from the 86–118°E SEIR data and, in this particular case, they may be ascribed to the earliest stages of breakup of Pangea (Dosso *et al.*, 1999). However, errorchron ages (mostly Sm–Nd) in the same general range also have been reported for oceanic areas that have had no known relation to continental breakup for many hundreds of millions or even more than a billion years; for example, for East Pacific Rise seamounts (Zindler *et al.*, 1984; Graham *et al.*, 1988; Niu *et al.*, 1996). Thus, a common interpretation of the ages implied by correlations of isotopic and parent–daughter ratios in MORB is that they represent a typical 'turnover', 'replenishment', or 'recycling' time of MORB asthenosphere in an open-system mantle. However, they may more likely just be a consequence of chemical equilibration times in a system undergoing mixing between different mantle reservoirs; if so, they have no particular chronological significance (Albarède, 2001). At present, we consider this explanation to be as viable for the 86–118°E SEIR as a Gondwanan-breakup connection.

CONCLUDING REMARKS

The distinctive Pb–Nd–Sr isotopic character of Indian MORB is generally attributed to the past incorporation and dispersal in the asthenosphere of material derived from old continental lithosphere and/or anciently subducted sediments (possibly, but not necessarily, delivered to the Indian MORB source region by mantle plumes) (e.g. see Mahoney *et al.*, 1992; Rehkämper & Hofmann, 1997). Among sampled parts of the Indian Ocean ridge system far from currently active hotspots, the comparatively low ε_{Nd} of much of the SEIR (Fig. 4) suggests that the eastern Indian Ocean asthenosphere may contain—or retain—slightly more such material, on average, than that beneath ridges farther west. Alternatively, the material that affected the sub-SEIR mantle had slightly lower average ε_{Nd} than that which affected the sources of sampled portions of the Central and Southwest Indian Ridges.

The Indian MORB isotopic signature has been proposed to be both a comparatively youthful feature, perhaps not much older than the early stages of the breakup of Gondwana (e.g. Storey *et al.*, 1988, 1989; Mahoney *et al.*, 1989, 1992; Weis & Frey, 1996), and a very ancient one (i.e. >1 Ga) (e.g. Hart, 1984; Dosso *et al.*, 1988; Crawford *et al.*, 1995). Studies of old Indian MORB and of Tethyan crust formed to the north of East Gondwana (Pyle *et al.*, 1995; Weis & Frey, 1996; Mahoney *et al.*, 1998; Zhang *et al.*, 2000) reveal that Indian-MORB-type isotopic compositions existed in places as long ago as the Late Jurassic in the Indian and southern Neo-Tethyan oceans, although they appear to have been distributed less uniformly than at present because some of the old basalts also lack Indian-MORB-type signatures, unlike the MORB in the main part of the Indian Ocean today. Regardless of whether the correlations in Fig. 7a–e reflect some type of mantle mixing or a widespread asthenospheric fractionation event associated with pre-breakup extension of Gondwanan lithosphere, the implied 200–300 Ma ages provide no evidence for an isotopic signature of truly great age in the mantle now beneath the 86–118°E SEIR. However, if the correlations do have any real time-significance, their *y*-intercepts suggest a source composition that would already have been slightly to moderately Indian-MORB-like 200–300 Myr ago. In turn, this would imply an age for the Indian-MORB-type signature in this portion of the mantle significantly greater than the maximum known age of the Kerguelen–Heard hotspot [$\sim$119 Ma (Pringle & Duncan, 2000) or possibly $\sim$135 Ma (Frey *et al.*, 1996)], which several workers have proposed to have been wholly or partly responsible for the introduction of the Indian MORB isotopic signature into the eastern Indian Ocean mantle (e.g. Storey *et al.*, 1988, 1989; Mahoney *et al.*, 1992; Weis & Frey, 1996). Both this consideration and the general lack of either a major Kerguelen–Heard or Amsterdam–St. Paul influence in 86–118°E MORB suggest that the effect of material derived from these hotspots on the composition of asthenosphere in the southeastern Indian Ocean is much smaller than believed previously.

ACKNOWLEDGEMENTS

We are grateful to K. Spencer, D. Pyle, Z. P. Yang, and N. Hulbirt for help with various aspects of the work onshore, and to the marine technicians and crew of the R.V. *Melville*, whose competence and dedication ensured the success of sampling operations at sea. We thank F. Frey for helpful comments, and J. Lupton for insightful discussions and access to the helium isotope laboratory (supported by the NOAA Vents program). B. Hanan, D. Weis, and an anonymous referee provided valuable critical reviews. W. White kindly permitted use of his unpublished data for Amsterdam and St. Paul. This study was supported by NSF-OCE grants to the four senior authors.

REFERENCES

Albarède, F. (2001). Radiogenic ingrowth in systems with multiple reservoirs: applications to the differentiation of the mantle–crust system. *Earth and Planetary Science Letters* **189**, 59–73.

Anderson, D. L. (2000). The statistics and distribution of helium in the mantle. *International Geology Reviews* **42**, 289–311.

Bach, W., Hegner, E., Erzinger, J. & Satir, M. (1994). Chemical and isotopic variations along the superfast spreading East Pacific Rise from 6°S to 30°S. *Contributions to Mineralogy and Petrology* **116**, 365–380.

Barling, J., Goldstein, S. L. & Nicholls, I. A. (1994). Geochemistry of Heard Island (southern Indian Ocean): characterization of an enriched mantle component and implications for enrichment of the sub-Indian Ocean mantle. *Journal of Petrology* **35**, 1017–1053.

Brooks, C., Hart, S. R., Hofmann, A. & James, D. E. (1976). Rb–Sr mantle isochrons from oceanic regions. *Earth and Planetary Science Letters* **32**, 51–61.

Castillo, P. R., Natland, J., Niu, Y. & Lonsdale, P. F. (1998). Sr, Nd and Pb isotopic variation along the Pacific–Antarctic risecrest, 53–57°S: implications for the composition and dynamics of the South Pacific upper mantle. *Earth and Planetary Science Letters* **154**, 109–125.

Castillo, P. R., Klein, E., Bender, J., Langmuir, C., Shirey, S., Batiza, R. & White, W. (2000). Petrology and Sr, Nd and Pb isotope geochemistry of MORB glasses from the 11°45′N to 15°00′N segment of the East Pacific Rise. *Geochemistry, Geophysics, Geosystems* **1**, 1999GC000024.

Christie, D. M., Mahoney, J. J., Frey, F. A., Graham, D. W., Danyushevsky, L. & Gregory, M. (1995). Cruise report, Westward Expedition of R.V. *Melville*, Leg 10. USA National Science Foundation.

Christie, D. M., West, B. P., Pyle, D. G. & Hanan, B. B. (1998). Chaotic topography, mantle flow and mantle migration in the Australian–Antarctic Discordance. *Nature* **394**, 637–644.

Church, S. E. & Tatsumoto, M. (1975). Lead isotope relations in oceanic ridge basalts from the Juan de Fuca–Gorda Ridge area, N.E. Pacific Ocean. *Contributions to Mineralogy and Petrology* **53**, 253–279.

Cochran, J. R., Sempéré, J.-C. & the SEIR Scientific Team (1997). The Southeast Indian Ridge between 88°E and 118°E: gravity anomalies and crustal accretion at intermediate spreading rates. *Journal of Geophysical Research* **102**, 15467–15487.

Coffin, M. F. & Rabinowitz, P. D. (1988). Evolution of the Conjugate East African–Madagascan Margins and the Western Somali Basin. Geological Society of America, Special Paper 2226, 78 pp.

Crawford, A. J., Briqueu, L., Laporte, C. & Hasenaka, T. (1955). Coexistence of Indian and Pacific oceanic upper mantle reservoirs beneath the central New Hebrides island arc. In: Taylor, B. & Natland, J. (eds) *Active Margins and Marginal Basins of the Western Pacific. Geophysical Monograph, American Geophysical Union* **88**, 199–217.

Davies, H. L., Sun, S.-S., Frey, F. A., Gautier, I., McCulloch, M. T., Price, R. C., Bassias, Y., Klootwijk, C. T. & Leclaire, L. (1989). Basalt basement from the Kerguelen Plateau and the trail of a Dupal plume. *Contributions to Mineralogy and Petrology* **103**, 457–469.

Doglioni, C. (1990). The global tectonic pattern. *Journal of Geodynamics* **12**, 21–38.

Dosso, L. & Rama Murthy, V. (1980). A Nd isotopic study of the Kerguelen Islands: inferences on enriched oceanic mantle sources. *Earth and Planetary Science Letters* **48**, 268–276.

Dosso, L., Vidal, P., Cantagrel, J. M., Lameyre, J., Marot, A. & Zimine, S. (1979). Kerguelen: continental fragment or oceanic island? Petrology and isotopic geochemistry evidence. *Earth and Planetary Science Letters* **43**, 46–60.

Dosso, L., Bougault, H., Beuzart, P., Calvez, J.-Y. & Joron, J.-L. (1988). The geochemical structure of the South-East Indian Ridge. *Earth and Planetary Science Letters* **88**, 47–59.

Dosso, L., Bougault, H., Langmuir, C., Bollinger, C., Bonnier, O. & Etoubleau, J. (1999). The age and distribution of mantle heterogeneity along the Mid-Atlantic Ridge (31–41°N). *Earth and Planetary Science Letters* **170**, 269–286.

Douglas-Priebe, L. M. (1998). Geochemical and petrogenetic effects of the interaction of the Southeast Indian Ridge and the Amsterdam–St. Paul hotspot. M.S. thesis, Oregon State University, Corvallis.

Duncan, R. A. & Storey, M. (1992). The life cycle of Indian Ocean hotspots. In: Duncan, R. A., Rea, D. K., Kidd, R. B., von Rad, U. & Weissel, J. K. (eds) *Synthesis of Results from Scientific Drilling in the Indian Ocean. Geophysical Monograph, American Geophysical Union* **70**, 91–103.

Frey, F. A., McNaughton, N. J., Nelson, D. R., deLaeter, J. R. & Duncan, R. A. (1996). Petrogenesis of the Bunbury Basalt, Western Australia: interaction between the Kerguelen plume and Gondwana lithosphere? *Earth and Planetary Science Letters* **144**, 163–183.

Frey, F. A., Weis, D., Borisova, A. Yu. & Xu, G. (2002). Involvement of continental crust in the formation of the Cretaceous Kerguelen Plateau: new perspectives from ODP Leg 120 sites. *Journal of Petrology* **43**, 1207–1239.

Galer, S. J. G. (1999). East Pacific Rise MORB through the Pb isotope looking glass (abstract). *EOS Transactions, American Geophysical Union* **80**, F1086.

Gautier, I., Weis, D., Mennessier, J.-P., Vidal, P., Giret, A. & Loubet, M. (1990). Petrology and geochemistry of Kerguelen basalts (South Indian Ocean): evolution of the mantle sources from ridge to an intraplate position. *Earth and Planetary Science Letters* **100**, 59–76.

Govindaraju, K. (1994). 1994 compilation of working values and sample description for 383 geostandards. *Geostandards Newsletter* **18**, 1–158.

Graham, D. W., Zindler, A., Kurz, M. D., Jenkins, W. J., Batiza, R. & Staudigel, H. (1988). He, Pb, Sr and Nd isotope constraints on magma genesis and mantle heterogeneity beneath young Pacific seamounts. *Contributions to Mineralogy and Petrology* **99**, 446–463.

Graham, D. W., Lupton, J., Klein, E., Christie, D. & Pyle, D. (1990). Helium isotope geochemistry of the Australian–Antarctic Discordance (abstract). *Seventh International Conference on Geochronology, Cosmochronology, and Isotope Geology, Geological Society of Australia* **27**, 41.

Graham, D. W., Jenkins, W. J., Schilling, J.-G., Thompson, G., Kurz, M. D. & Humphris, S. E. (1992). Helium isotope geochemistry of mid-ocean ridge basalts from the South Atlantic. *Earth and Planetary Science Letters* **110**, 133–147.

Graham, D. W., Johnson, K. T. M., Douglas-Priebe, L. & Lupton, J. E. (1999). Hotspot–ridge interaction along the Southeast Indian Ridge near Amsterdam and St. Paul islands: helium isotope evidence, *Earth and Planetary Science Letters* **167**, 297–310.

Graham, D. W., Lupton, J. E., Spera, F. J. & Christie, D. M. (2001). Upper mantle dynamics revealed through spatial analysis of helium isotope variations along the Southeast Indian Ridge. *Nature* **409**, 701–703.

Hamelin, B. & Allègre, C. J. (1985). Large-scale regional units in the depleted upper mantle revealed by an isotope study of the South-West Indian Ridge. *Nature* **315**, 196–199.

Hamelin, B., Dupré, B. & Allègre, C. J. (1986). Pb–Sr–Nd isotopic data of Indian Ocean Ridges: new evidence of large-scale mapping of mantle heterogeneities. *Earth and Planetary Science Letters* **76**, 288–298.

Hanan, B. B. & Graham, D. W. (1996). Lead and helium isotope evidence from oceanic basalts for a common deep source of mantle plumes. *Science* **272**, 991–995.

Hanan, B. B., Pyle, D. G., Blichert-Toft, J., Christie, D. & Albarède, F. (2000). Ultra-depleted hafnium isotopes from Australian–Antarctic Discordance MORB (abstract). *V.M. Goldschmidt Conference Abstracts* **5**, 478.

Hart, S. R. (1984). A large-scale isotope anomaly in the Southern Hemisphere mantle. *Nature* **309**, 753–757.

Hedge, C. E., Futa, K., Engel, C. G. & Fisher, R. L. (1979). Rare earth abundances and Rb–Sr systematics of basalts, gabbro, anorthosite and minor granitic rocks from the Indian Ocean ridge system,

Western Indian Ocean. *Contributions to Mineralogy and Petrology* **68**, 373–376.

Hilton, D. R., Barling, J. & Wheller, G. E. (1995). Effect of shallow-level contamination on the helium isotope systematics of ocean-island lavas. *Nature* **373**, 330–333.

Ingle, S., Weis, D. & Frey, F. A. (2002). Indian continental crust recovered from Elan Bank, Kerguelen Plateau (ODP Leg 183, Site 1137). *Journal of Petrology* **43**, 1241–1257.

Ito, E., White, W. M. & Göpel, C. (1987). The O, Sr, Nd and Pb isotope geochemistry of MORB. *Chemical Geology* **62**, 157–176.

Johnson, K. T. M., Scheirer, D. S., Forsyth, D. W. & Graham, D. W. (1996). Cruise report, Boomerang Expedition, Leg 06, R.V. *Melville*. USA National Science Foundation.

Johnson, K. T. M., Graham, D. W., Rubin, K. H., Nicolaysen, K., Scheirer, D. S., Forsyth, D. W., Baker, E. T. & Douglas-Priebe, L. M. (2000). Boomerang Seamount: the active expression of the Amsterdam–St. Paul hotspot, Southeast Indian Ridge. *Earth and Planetary Science Letters* **183**, 245–259.

Klein, E. M. & Langmuir, C. H. (1987). Global correlations of ocean ridge basalt chemistry with axial depth and crustal thickness. *Journal of Geophysical Research* **92**, 8089–8115.

Klein, E. M., Langmuir, C. H., Zindler, A., Staudigel, H. & Hamelin, B. (1988). Isotope evidence of a mantle convection boundary at the Australian–Antarctic Discordance. *Nature* **333**, 623–629.

Lawver, L. A. & Gahagan, L. M. (1993). Subduction zones, magmatism, and the breakup of Pangea. In: Stone, D. B. & Runcorn, S. K. (eds) *Flow and Creep in the Solar System: Observations, Modeling and Theory*. Dordrecht: Kluwer Academic, pp. 225–247.

le Roex, A. P., Dick, H. J. B., Erlank, A. J., Reid, A. M., Frey, F. A. & Hart, S. R. (1983). Geochemistry, mineralogy and petrogenesis of lavas erupted along the Southwest Indian Ridge between the Bouvet triple junction and 11°E. *Journal of Petrology* **24**, 267–318.

Luyendyk, B. P. & Rennick, W. (1977). Tectonic history of aseismic ridges in the eastern Indian Ocean. *Bulletin of the Geological Society of America* **88**, 1347–1356.

Mahoney, J. J., Natland, J. H., White, W. M., Poreda, R., Bloomer, S. H., Fisher, R. L. & Baxter, A. N. (1989). Isotopic and geochemical provinces of the western Indian Ocean spreading centers. *Journal of Geophysical Research* **94**, 4033–4052.

Mahoney, J. J., le Roex, A. P., Peng, Z. X., Fisher, R. L. & Natland, J. H. (1992). Southwestern limits of Indian Ocean ridge mantle and the origin of low-$^{206}Pb/^{204}Pb$ mid-ocean ridge basalt: isotope systematics of the central Southwest Indian Ridge (17°–50°E). *Journal of Geophysical Research* **97**, 19771–19790.

Mahoney, J. J., Sinton, J. M., Kurz, M. D., Macdougall, J. D., Spencer, K. J. & Lugmair, G. W. (1994). Isotope and trace element characteristics of a super-fast spreading ridge: East Pacific Rise, 13–23°S. *Earth and Planetary Science Letters* **121**, 173–193.

Mahoney, J. J., Jones, W. B., Frey, F. A., Salters, V. J. M., Pyle, D. G. & Davies, H. L. (1995). Geochemical characteristics of lavas from Broken Ridge, the Naturaliste Plateau and southernmost Kerguelen Plateau: Cretaceous plateau volcanism in the southeast Indian Ocean. *Chemical Geology* **120**, 315–345.

Mahoney, J. J., Frei, R., Tejada, M. L. G., Mo, X. X., Leat, P. T. & Nägler, T. F. (1998). Tracing the Indian Ocean mantle domain through time: isotopic results from old West Indian, East Tethyan, and South Pacific seafloor. *Journal of Petrology* **39**, 1285–1306.

Marks, K. M., Sandwell, D. T., Vogt, P. R. & Hall, S. A. (1991). Mantle downwelling beneath the Australian–Antarctic Discordance zone: evidence from geoid height versus topography. *Earth and Planetary Science Letters* **103**, 325–338.

Michard, A., Montigny, R. & Schlich, R. (1986). Geochemistry of the mantle below the Rodriguez triple junction and the South-East Indian Ridge. *Earth and Planetary Science Letters* **78**, 104–114.

Neal, C. R., Mahoney, J. J. & Chazey, W. J., III (2002). Mantle sources and the highly variable role of continental lithosphere in basalt petrogenesis of the Kerguelen Plateau and Broken Ridge LIP: results from ODP Leg 183. *Journal of Petrology* **43**, 1177–1205.

Nicolaysen, K., Frey, F. A., Kurz, M. D., Weis, D., Leyrit, H. & Giret, A. (1998). $^{3}He/^{4}He$ ratios in Kerguelen Archipelago basalts: new evidence for an undegassed mantle plume component (abstract). *Mineralogical Magazine* **62**, 1083–1084.

Niu, Y. & Batiza, R. (1997). Trace element evidence from seamounts for recycled oceanic crust in the Eastern Pacific mantle. *Earth and Planetary Science Letters* **148**, 471–483.

Niu, Y., Waggoner, D. G., Sinton, J. M. & Mahoney, J. J. (1996). Mantle source heterogeneity and melting processes beneath seafloor spreading centers: the East Pacific Rise, 18°–19°S. *Journal of Geophysical Research* **101**, 27711–27733.

Poreda, R. J., Schilling, J.-G. & Craig, H. (1993). Helium isotope ratios in Easter Microplate basalts. *Earth and Planetary Science Letters* **119**, 319–329.

Price, R. C., Kennedy, A. K., Riggs-Sneeringer, M. & Frey, F. A. (1986). Geochemistry of basalts from the Indian Ocean triple junction: implications for the generation of Indian Ocean ridge basalts. *Earth and Planetary Science Letters* **78**, 379–396.

Pringle, M. S. & Duncan, R. A. (2000). Basement ages from the southern and central Kerguelen Plateau: initial products of the Kerguelen large igneous province (abstract). *EOS Transactions, American Geophysical Union* **81**, S424.

Pyle, D. G., Christie, D. M. & Mahoney, J. J. (1992). Resolving an isotopic boundary within the Australian–Antarctic Discordance. *Earth and Planetary Science Letters* **112**, 161–178.

Pyle, D. G., Christie, D. M., Mahoney, J. J. & Duncan, R. A. (1995). Geochemistry and geochronology of ancient southeast Indian and southwest Pacific seafloor. *Journal of Geophysical Research* **100**, 22261–22282.

Rehkämper, M. & Hofmann, A. W. (1997). Recycled oceanic crust and sediment in Indian Ocean MORB. *Earth and Planetary Science Letters* **147**, 91–106.

Ricard, Y., Doglioni, C. & Sabadini, R. (1991). Differential rotation between lithosphere and mantle: a consequence of lateral viscosity variations. *Journal of Geophysical Research* **96**, 8407–8415.

Rousseeuw, P. J. & Leroy, A. M. (1987). *Robust Regression and Outlier Detection*. New York: John Wiley, 329 pp.

Salters, V. J. M. & White, W. M. (1998). Hf isotope constraints on mantle evolution. *Chemical Geology* **145**, 447–460.

Salters, V. J. M., Storey, M., Sevigny, J. H. & Whitechurch, H. (1992). Trace element and isotopic characteristics of Kerguelen–Heard plateau basalts. In: Wise, S. W., Schlich, R., Julson, A. *et al.* (eds) *Proceedings of the Ocean Drilling Program, Scientific Results*, 120. College Station, TX: Ocean Drilling Program, pp. 55–62.

Saunders, A. D., Storey, M., Gibson, I. L., Leat, P., Hergt, J. & Thompson, R. N. (1991). Chemical and isotopic constraints on the origin of basalts from Ninetyeast Ridge, Indian Ocean: results from DSDP Legs 22 and 26 and ODP Leg 121. In: Weissel, J., Peirce, J., Taylor, E., Taylor, E. *et al.* (eds) *Proceedings of the Ocean Drilling Program, Scientific Results*, 121. College Station, TX: Ocean Drilling Program, pp. 559–590.

Scheirer, D. S., Forsyth, D. W., Conder, J. A., Eberle, M. A., Hung, S.-H., Johnson, K. T. M. & Graham, D. W. (2000). Anomalous seafloor spreading of the Southeast Indian Ridge near the Amsterdam–St. Paul Plateau. *Journal of Geophysical Research* **105**, 8243–8262.

Schilling, J.-G. (1985). Upper mantle heterogeneities and dynamics. *Nature* **314**, 62–67.

Schilling, J.-G., Kingsley, R., Fontignie, D., Poreda, R. & Xue, S. (1999). Dispersion of the Jan Mayen and Iceland mantle plumes in the Arctic: a He–Pb–Nd–Sr isotope tracer study of basalts from the Kolbeinsey, Mohns, and Knipovich ridges. *Journal of Geophysical Research* **104**, 10543–10569.

Sempéré, J.-C., Cochran, J. R. & the SEIR Scientific Team (1997). The Southeast Indian Ridge between 88°E and 118°E: variations in crustal accretion at constant spreading rate. *Journal of Geophysical Research* **102**, 15489–15505.

Small, C. (1995). Observations of ridge–hotspot interactions in the Southern Ocean. *Journal of Geophysical Research* **100**, 17931–17946.

Small, C. & Sandwell, D. T. (1994). Imaging mid-ocean ridge transitions with satellite gravity. *Geology* **22**, 123–126.

Smith, A. D. & Lewis, C. (1999). The planet beyond the plume hypothesis. *Earth-Science Reviews* **42**, 135–182.

Smith, W. H. F. & Sandwell, D. T. (1997). Global sea floor topography from satellite altimetry and ship depth soundings. *Science* **277**, 1956–1962.

Storey, M., Saunders, A. D., Tarney, J., Leat, P. T., Thirlwall, M. F., Thompson, R. N., Menzies, M. A. & Marriner, G. F. (1988). Geochemical evidence for plume–mantle interactions beneath Kerguelen and Heard islands, Indian Ocean. *Nature* **336**, 371–374.

Storey, M., Saunders, A. D., Tarney, J., Gibson, I. L., Norry, M. J., Thirlwall, M. F., Leat, P. T., Thompson, R. N. & Menzies, M. A. (1989). Contamination of Indian Ocean asthenosphere by the Kerguelen–Heard mantle plume. *Nature* **338**, 574–576.

Sturm, M. E., Klein, E. M., Graham, D. W. & Karsten, J. K. (1999). Age constraints on crustal recycling to the mantle beneath the southern Chile Ridge: He–Pb–Sr–Nd isotope systematics. *Journal of Geophysical Research* **104**, 5097–5114.

Sun, S.-S. (1980). Lead isotopic study of young volcanic rocks from mid-ocean ridges, ocean islands, and island arcs. *Philosophical Transactions of the Royal Society of London, Series A* **297**, 4009–4045.

Todt, W., Cliff, R. A., Hanser, A. & Hofmann, A. W. (1996). Evaluation of a $^{202}Pb + {}^{205}Pb$ double spike for high-precision lead isotopic analyses. In: Basu, A. & Hart, S. (eds) *Earth Processes: Reading the Isotopic Code. Geophysical Monograph, American Geophysical Union* **95**, 429–437.

Valbracht, P. J., Honda, M., Matsumoto, T., Mattielli, N., McDougall, I., Ragettli, R. & Weis, D. (1996). Helium, neon and argon isotope systematics in Kerguelen ultramafic xenoliths: implications for mantle source signatures. *Earth and Planetary Science Letters* **138**, 29–38.

Verma, S. P., Schilling, J.-G. & Waggoner, D. G. (1983). Neodymium isotopic evidence for Galapágos hotspot–spreading centre system evolution. *Nature* **306**, 654–657.

Vlastélic, I., Dosso, L., Bougault, H., Aslanian, D., Géli, L., Etoubleau, J., Bohn, M., Joron, J.-L. & Bollinger, C. (2000). Chemical systematics of an intermediate spreading ridge: the Pacific–Antarctic Ridge between 56°S and 66°S. *Journal of Geophysical Research* **105**, 2915–2936.

Weis, D. & Frey, F. A. (1996). Role of the Kerguelen plume in generating the eastern Indian Ocean seafloor. *Journal of Geophysical Research* **101**, 13831–13849.

Weis, D., Bassias, Y., Gautier, I. & Mennessier, J.-P. (1989). Dupal anomaly in existence 115 Ma ago: evidence from isotopic study of the Kerguelen Plateau (South Indian Ocean). *Geochimica et Cosmochimica Acta* **53**, 2125–2131.

Weis, D., Frey, F. A., Leyrit, H. & Gautier, I. (1993). Kerguelen Archipelago revisited: geochemical and isotopic study of the Southeast Province lavas. *Earth and Planetary Science Letters* **118**, 101–119.

Weis, D., Frey, F. A., Giret, A. & Cantagrel, J.-M. (1998). Geochemical characteristics of the youngest volcano (Mount Ross) in the Kerguelen Archipelago: inferences for magma flux, lithosphere assimilation and composition of the Kerguelen plume. *Journal of Petrology* **39**, 973–994.

Weis, D., Frey, F. A., Schlich, R., Schaming, M., Montigny, R., Damasceno, D., Mattielli, N., Nicolaysen, K. E. & Scoates, J. S. (2002). Trace of the Kerguelen mantle plume from seamounts between the Kerguelen Archipelago and Heard Island, Indian Ocean. *Geochemical and Geophysical Geosystems*, in press.

West, B. P., Wilcock, W. S. D., Sempéré, J.-C. & Géli, L. (1997). Three-dimensional structure of asthenospheric flow beneath the Southeast Indian Ridge. *Journal of Geophysical Research* **102**, 7783–7802.

White, W. M. (1993). $^{238}U/^{204}Pb$ in MORB and open system evolution of the depleted mantle. *Earth and Planetary Science Letters* **115**, 211–226.

Yang, H.-J., Frey, F. A., Weis, D., Giret, A., Pyle, D. & Michon, G. (1998). Petrogenesis of the flood basalts forming the northern Kerguelen Archipelago: implications for the Kerguelen plume. *Journal of Petrology* **39**, 711–748.

Zhang, S.-Q., Mahoney, J. J., Mo, X. X., Ghazi, A. M., Milani, L., Crawford, A. J., Guo, T.-Y. & Zhao, Z.-D. (2000). Evidence for a widespread Neo-Tethyan upper mantle with Indian-MORB-type isotopic signatures (abstract). *EOS Transactions, American Geophysical Union* **81**, F1356.

Zindler, A., Staudigel, H. & Batiza, R. (1984). Isotope and trace element geochemistry of young Pacific seamounts: implications for the scale of upper mantle heterogeneity. *Earth and Planetary Science Letters* **70**, 175–195.